Evidence for Decreased Precipitation Variability in the Yucatán Peninsula During the Mid-Holocene

Gabriela Serrato Marks[1,2] [ID], **Martín Medina-Elizalde[3]** [ID], **Stephen Burns[3]**, **Syee Weldeab[4]** [ID], **Fernanda Lases-Hernandez[5]** [ID], **Gabriela Cazares[1]** [ID], and **David McGee[1]** [ID]

[1]Department of Earth, Atmospheric, and Planetary Sciences (EAPS), Massachusetts Institute of Technology, Cambridge, MA, USA, [2]Marine Geology and Geophysics Department, Woods Hole Oceanographic Institution, Woods Hole, MA, USA, [3]Department of Geosciences, University of Massachusetts Amherst, Amherst, MA, USA, [4]Department of Earth Science, University of California, Santa Barbara, CA, USA, [5]Facultad de Química, Unidad Sisal, Universidad Nacional Autónoma de México, Puerto de Abrigo, Sisal, Yucatán, México

Abstract The Yucatán Peninsula (YP) has a complex hydroclimate with many proposed drivers of interannual and longer-term variability, ranging from coupled ocean–atmosphere processes to frequency of tropical cyclones. The mid-Holocene, a time of higher Northern Hemisphere summer insolation, provides an opportunity to test the relationship between YP precipitation and ocean temperature. Here, we present a new, ~annually resolved speleothem record of stable isotope ($\delta^{18}O$ and $\delta^{13}C$) and trace element (Mg/Ca and Sr/Ca) ratios for a section of the mid-Holocene (5.2–5.7 kyr BP), before extensive agriculture began in the region. A meter-long stalagmite from Río Secreto, a cave system in Playa del Carmen, Mexico, was dated using U–Th geochronology and layer counting, yielding multidecadal age uncertainty (median 2SD of ±70 years). New proxy data were compared to an existing late Holocene stalagmite record from the same cave system, allowing us to examine changes in hydrology over time and to paleoclimate records from the southern YP. The $\delta^{18}O$, $\delta^{13}C$, and Mg/Ca data consistently indicate higher mean precipitation and lower precipitation variability during the mid-Holocene compared to the late Holocene. Despite this reduced variability, multidecadal precipitation variations were persistent in regional hydroclimate during the mid-Holocene. We therefore conclude that higher summer insolation led to increased mean precipitation and decreased precipitation variability in the northern YP but that the region is susceptible to dry periods across climate mean states. Given projected decreases in wet season precipitation in the YP's near future, we suggest that climate mitigation strategies emphasize drought preparation.

Plain Language Summary We present a new record of past climate from the Yucatán Peninsula (YP). We used a stalagmite that grew in Playa del Carmen, Mexico, from around 5,700 years ago to 5,200 years ago, part of the mid-Holocene. We wanted to test the relationship between YP precipitation and ocean temperature, which is important due to projected decreases in wet season precipitation. The stalagmite also recorded climate conditions before extensive agriculture began in the region. We collected geochemical data from the stalagmite to act as proxies for past climate. Then, we compared the data to both a younger stalagmite from the same cave and other records from the southern YP. The geochemical data suggest that there was more rain and lower rainfall variability during the mid-Holocene compared to the late Holocene (more recently). Despite reduced precipitation variability, droughts and wet periods still occurred. We therefore conclude that the region is susceptible to dry periods, even during wetter climate conditions, and suggest that climate change mitigation strategies emphasize drought preparation.

1. Introduction

The Yucatán Peninsula (YP) harbors diverse ecosystems, including the Mesoamerican barrier reef and tropical rainforests, and has been inhabited by Maya societies for thousands of years. Biological systems and human societies in the region developed under limited surface and groundwater availability and have therefore been vulnerable to hydroclimate extremes. Under future climate warming scenarios, the YP is projected to receive less wet season precipitation compared to current precipitation (Karmalkar et al., 2011). The important role of hydroclimate variability in shaping the past, present, and future of human societies and

ecosystems motivates efforts to better document past hydroclimate changes in the YP and their relationships to regional conditions and external forcings.

There has been extensive research on the potential drivers of YP climate variability during the Common Era (CE; past 2,000 years) and on the role of drought in the decline of Maya civilization during the Preclassic (droughts at ~180 and 240 CE) and Terminal Classic Periods (750–950 CE) (e.g., Curtis et al., 1996; Hodell et al., 1995; Medina-Elizalde, Burns, et al., 2016; Medina-Elizalde et al., 2010). Climate simulations and paleoclimate records suggest that late Holocene precipitation in the YP was linked to North Atlantic climate variability. Potential controls on precipitation amount include changes in sea surface temperature (SST), sea level pressure (SLP) (Bhattacharya et al., 2017), tropical cyclone variability (Frappier et al., 2007, 2014; Medina-Elizalde, Burns, et al., 2016), and the mean position of the Intertropical Convergence Zone (ITCZ) (e.g., Bush et al., 2009; Lechleitner et al., 2017; Pollock et al., 2016; Ridley et al., 2015). These climate variations are likely linked, further complicating diagnostics (McGee et al., 2014). YP precipitation variability also suggests a link with El Niño–Southern Oscillation (ENSO) in the Pacific (Frappier et al., 2014; Giannini et al., 2000; Lachniet et al., 2017; Medina-Elizalde, Burns, et al., 2016; Medina-Elizalde, Polanco-Martínez, et al., 2016, Medina-Elizalde et al., 2017; Metcalfe et al., 2009; Pollock et al., 2016; Stahle et al., 2012).

The mid-Holocene is of particular interest to investigate the role of external forcing on hydroclimate variability in the Caribbean region. During the mid-Holocene, solar radiation was higher in the Northern Hemisphere (NH) during the boreal summer relative to the late Holocene and present (Hoddell et al., 1995; Laskar et al., 2004) and ENSO variability was markedly decreased (Carré et al., 2014; Chen et al., 2016; Emile-Geay et al., 2016). Limited data on Atlantic and Caribbean SSTs are available for this time period, but paleotemperature reconstructions indicate that global temperatures reached a local maximum around 6,500 years before present (Kaufman et al., 2020). Based on increased NH summer radiation during the mid-Holocene, it is possible that there was stronger seasonality and higher summer SSTs in the North Atlantic and Caribbean (Marcott et al., 2013; Marsicek et al., 2018). Given modern connections between the North Atlantic and Caribbean hydroclimate (e.g., Bhattacharya et al., 2017) and previous paleo research in the southern YP (e.g., Pollock et al., 2016; Wahl et al., 2014; Winter et al., 2020), we expect that the mid-Holocene northern YP was wetter and less variable in precipitation than the late Holocene or the present.

Data from speleothems and sediment cores in the southern YP are broadly consistent with the expectation of wetter mid-Holocene conditions (e.g., Pollock et al., 2016; Wahl et al., 2014; Winter et al., 2020). However, existing paleoclimate records do not address the northeast YP, which is drier than the southern YP at present, nor do they offer a consensus regarding the magnitude and frequency of precipitation variability during the Holocene. Published paleoclimate records in the YP are based on proxy data from various archives, including speleothems (e.g., Akers et al., 2016; Frappier et al., 2014; Pollock et al., 2016, Winter et al., 2020) and lake, sinkhole, wetland, and swamp sediment cores (Anderson & Wahl, 2016; Curtis et al., 1996; Douglas et al., 2015; Gutiérrez-Ayala et al., 2012; Hodell et al., 2005; Metcalfe et al., 2009; Rosenmeier et al., 2002; Roy et al., 2017). Therefore, there is a rich body of work that serves as a foundation for further studies.

Although there are several valuable paleoclimate records available in the YP region (recent examples include Kennett et al., 2012; Medina-Elizalde et al., 2010, Pollock et al., 2016; Richey et al., 2009, Ridley et al., 2015, Wahl et al., 2014; Winter et al., 2020), many existing archives do not have high enough temporal resolution (and low enough age uncertainty) to investigate interannual to decadal hydroclimate variability in the region. Furthermore, the majority of the existing records come from Belize and Guatemala (e.g., Pollock et al., 2016; Wahl et al., 2014; Winter et al., 2020), so there is a paucity of data from the northern YP, including parts of present-day Mexican states of Quintana Roo, Campeche, and Yucatán. Winter et al. (2020) highlight the importance of considering the late versus mid-Holocene with sufficient complexity—despite existing data, more granular records (spatially and temporally) are beneficial. Therefore, there is a need for climate archives with high temporal resolution from the northern YP to investigate changes in climate variability in the mid-Holocene.

In order to refine our understanding of hydroclimate variability in the YP and its underlying drivers during the mid-Holocene, we present stalagmite $\delta^{18}O$, $\delta^{13}C$, Mg/Ca, and Sr/Ca records spanning the interval between 5.2 and 5.7 kyr before present (BP). The stalagmite we use, named RS1, was collected in April 2013 from an isolated chamber in the Río Secreto (RS) cave system, located in the northeastern YP (Figure 1a).
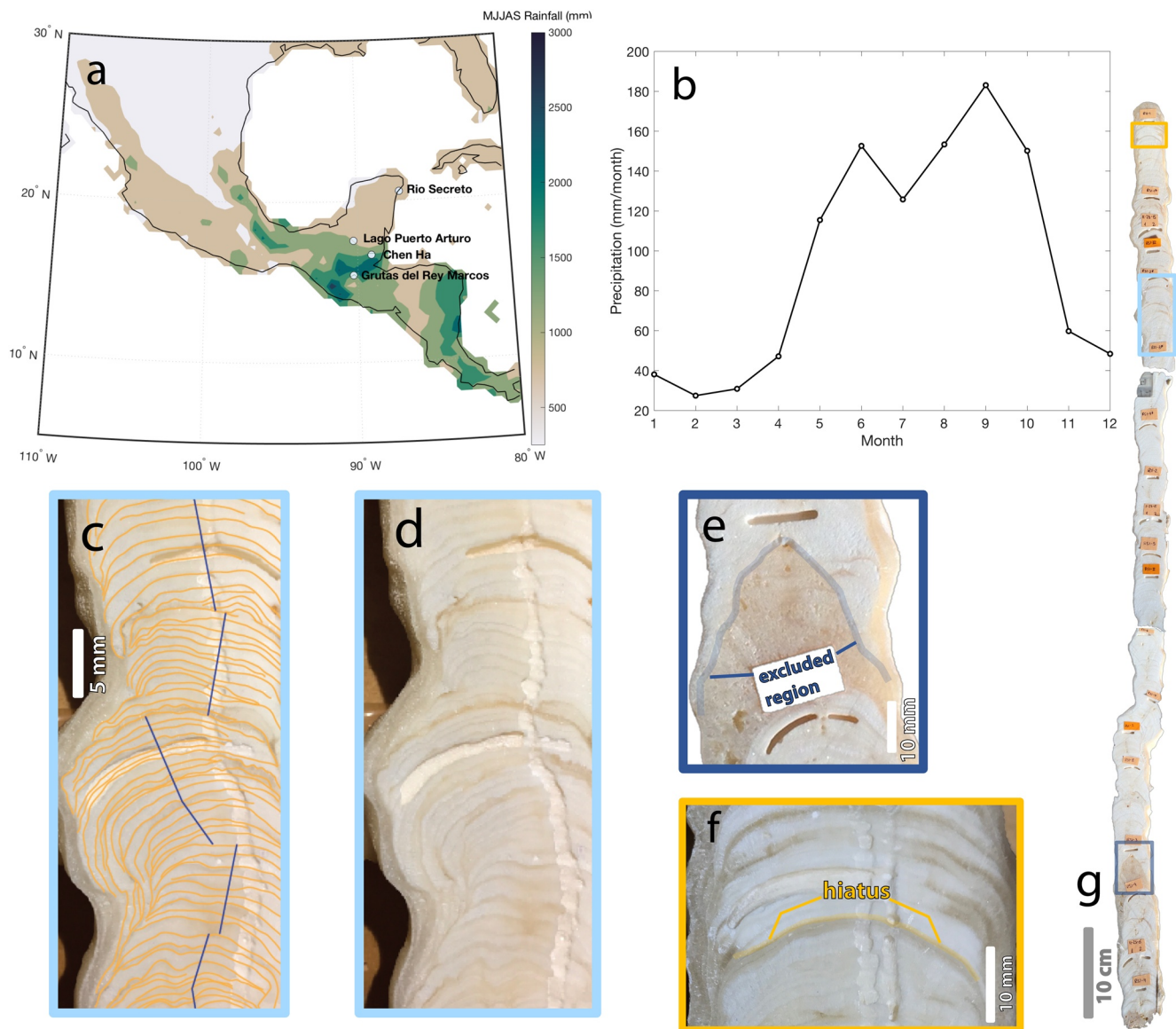
Figure 1. (a) Total rainfall from the summer wet season (MJJAS) in Central America and the Yucatán Peninsula, averaged yearly. Circles indicate study sites: Río Secreto cave (this work), Lago Puerto Arturo (Wahl et al., 2014), Chen Ha (Pollock et al., 2016), and Grutas del Rey Marcos (Winter et al., 2020). (b) Monthly precipitation in the 0.5° × 0.5° grid cell closest to Río Secreto. Rainfall data in (a) and (b) are from the Centro de Ciencias de la Atmósfera at the Universidad Nacional Autónoma de México (UNAM) v0705 data set, 1950–2002 (Mendez & Caetano, 2007). (c) Detail of mm-scale layers. Individual layers (orange) are deposited from bottom to top, with visible changes in thickness over time and changes in growth axis (straight lines). (d) Same as (c), without annotations. (e) Darker region without visible layers (surrounding the white rectangle); the region and the white segment below it were not used in this paper. (f) Potential hiatus near the top of RS1. (g) Full stalagmite. Colored boxes indicate location of images shown in (c)–(f).

An extensive drip water monitoring system was installed in 2014; RS1 was sampled closest to Drip Station A referenced in Lases-Hernandez et al. (2019). RS1 is a ~1-m tall calcite stalagmite, which was partially collapsed at the time of collection. It presents visually distinct lamination, allowing development of an age model based on laminae counting and U-series dating (see Section 2). Stalagmite $\delta^{18}O$ and $\delta^{13}C$ have often been used to infer changes in precipitation in this region (e.g., Medina-Elizalde et al., 2010; Pollock et al., 2016; Ridley et al., 2015), while Mg/Ca and Sr/Ca have not been examined previously in the YP but have been interpreted to reflect precipitation amount in other settings.

This study examines the new stalagmite record in comparison to another stalagmite-based precipitation record, known as Itzamna, from the same well-studied cave, spanning ~3–1.6 kyr BP (Medina-Elizalde,

Burns, et al., 2016). Stalagmite proxy records from the same location allow us to contrast inferred mid-Holocene and late Holocene hydroclimate variability despite the limited growth interval of each individual sample and decrease the uncertainty associated with comparing stalagmite proxy records from different locations and cave environments. Furthermore, this research focuses on a site located north of existing records, in present-day Quintana Roo (Figure 1a).

1.1. Regional Climate

The whole YP experiences a strong seasonality in precipitation amount (Figure 1b), with over 90% of rainfall occurring between April and December in the southern YP (Anderson & Wahl, 2016). The rainy season occurs in the summer and is often interrupted by decreased rainfall in July or August (Anderson & Wahl, 2016; Karmalkar et al., 2011; Lases-Hernandez et al., 2019; Muñoz et al., 2008). About 70% of annual rainfall occurs between June and November (Medina-Elizalde, Polanco-Martínez, et al., 2016). Maximum precipitation often occurs in September, when the ITCZ is at its northernmost position and Atlantic tropical cyclone frequency peaks (Kovacs et al., 2017; Lases-Hernandez et al., 2019) (Figure 1b). Strong easterly winds, known as the Caribbean Low Level Jet (CLLJ), bring moisture from the warm Caribbean Sea to the YP (Karmalkar et al., 2011; Muñoz et al., 2008); if enhanced, the CLLJ drives increased moisture transport and convergence in the region (Karmalkar et al., 2011; Mestas-Nuñez et al., 2007; Muñoz et al., 2008). The large-scale structure of the vertically integrated water vapor fluxes associated with the CLLJ links the Caribbean and Gulf of Mexico regions to climate regimes in the US, particularly during boreal summer (Mestas-Nuñez et al., 2007; Muñoz et al., 2008). We note that historical precipitation variability in the YP region is linked to that of the broader Caribbean region, particularly the northern sector, as indicated by spatial–temporal correlation analyses of instrumental precipitation records (e.g., Medina-Elizalde et al., 2017). In addition, it is important to note that up to 20% of cumulative western North Atlantic annual precipitation comes from tropical cyclones (Larson et al., 2005); this indicates that tropical cyclones play an important role in YP precipitation amount.

Within the YP, there are differences in precipitation amount; this is part of the motivation for new paleo records from a less-studied area of the YP. Monthly climatology from 1901 to 2002 reveals that Playa del Carmen, where RS1 was collected, receives significantly less total wet season rainfall than other recently studied sites in the southern YP (Pollock et al., 2016; Wahl et al., 2014; Winter et al., 2020) (Figure 1a). However, RS is also more influenced by tropical storms than are the other sites; a study comparing all the Mexican states noted that Quintana Roo had the highest number of tropical cyclone landfalls on the east coast of Mexico from 1970 to 2010 (Farfán et al., 2014). Our analysis of historical (1842–2020 CE) storm tracks at each site indicated that there were 67 tropical cyclones near RS, 33 each at Chen Ha (Pollock et al., 2016) and Lago Puerto Arturo (Wahl et al., 2014), and 9 at Grutas del Rey Marcos (Winter et al., 2020) within 60 nautical miles of each site (Knapp et al., 2010, 2018; Landsea & Franklin, 2013); this analysis included tropical storms through Category 5 hurricanes but not extratropical storms or tropical depressions. Climate models based on future emissions scenarios indicate that tropical cyclone landfalls may increase in the YP (Appendini et al., 2019), though another study predicted lower wet season precipitation in the YP (Karmalkar et al., 2011). Due to the current frequency of tropical storms in the northeastern YP, it is important to have more climate data from this highly vulnerable region.

1.2. Climate Proxies

Stalagmite $\delta^{18}O$ records in Mesoamerica, including the YP, are interpreted to reflect changes in precipitation amount (e.g., Akers et al., 2016; Lachniet et al., 2017; Medina-Elizalde, Burns, et al., 2016; Medina-Elizalde, Polanco-Martínez, et al., 2016), with more negative $\delta^{18}O$ values indicating increased precipitation, as expected from an amount effect, or the empirical relationship between precipitation amount and $\delta^{18}O$ composition observed in the tropics from seasonal to interannual time scales (Burns et al., 1998; Dansgaard, 1964; Lases-Hernandez et al., 2019; Vuille et al., 2003). Changes in $\delta^{13}C$ in stalagmites reflect a number of local processes associated with the soil cover, epikarst, and vadose zone (Genty et al., 2006). Some of the most common controls include the ratio of C3 to C4 vegetation above the cave (Burns et al., 2016; Dorale et al., 1998) and the amount of degassing in the vadose zone (Lachniet et al., 2004). Rainfall amount can influence drip water $\delta^{13}C$ (and therefore stalagmite $\delta^{13}C$) by affecting soil moisture and organic matter

production, bedrock dissolution, degassing, and prior calcite precipitation (PCP) (Genty et al., 2006; Ridley et al., 2015; Wong & Breecker, 2015).

In low-latitude caves where the overlying vegetation is expected to remain relatively stable over time, stalagmite $\delta^{13}C$ variability can reflect precipitation amount in the Central American region, as observed in Belize (Ridley et al., 2015). Low precipitation enhances degassing and PCP, increases bedrock carbon contributions, and decreases soil bio-productivity, all ultimately increasing drip water $\delta^{13}C$ and stalagmite $\delta^{13}C$ (e.g., Pollock et al., 2016; Ridley et al., 2015). In the YP, we assume that the type of vegetation remained relatively constant over the ~500 years captured in this research or that the effects of vegetation changes were substantially smaller than those of precipitation changes; this is a reasonable assumption because we focus on the mid-Holocene, before extensive deforestation and maize agriculture (Anderson & Wahl, 2016; Aragón-Moreno et al., 2012; Islebe et al., 2018). Furthermore, sediment core studies from Guatemala indicate that there was persistent closed canopy forest during the mid-Holocene, despite the relatively high occurrence of natural or human-generated fires (Anderson & Wahl, 2016.) Therefore, we will use stalagmite $\delta^{13}C$ as a proxy for moisture availability in RS1.

Although stalagmite $\delta^{18}O$ and $\delta^{13}C$ records have been widely interpreted as hydroclimate proxies, they are not without complexities. Stalagmite $\delta^{18}O$ can be influenced by changes in moisture source and upstream water vapor history. Similarly, stalagmite $\delta^{13}C$ can be impacted by soil and karst processes not directly related to precipitation variability (Genty et al., 2001; Hellstrom et al., 1998). Moreover, both $\delta^{18}O$ and $\delta^{13}C$ can also be affected by kinetic fractionation, especially in low humidity environments. Despite these potentially complicating issues, previous studies in the YP and Belize present multiple lines of evidence that stalagmite $\delta^{18}O$ and $\delta^{13}C$ can record local and regional precipitation amount (Medina-Elizalde, Burns, et al., 2016; Medina-Elizalde, Polanco-Martínez, et al., 2016; Medina-Elizalde et al., 2010, 2017; Pollock et al., 2016; Ridley et al., 2015). We analyze Mg/Ca and Sr/Ca ratios to examine their magnitude and frequency variability and to test interpretations from the more conventional $\delta^{18}O$ and $\delta^{13}C$ records. This is the first study that examines Mg/Ca and Sr/Ca ratios in a stalagmite from the YP region.

Many stalagmite analyses in other locations have applied Mg/Ca and Sr/Ca for hydroclimate reconstruction (e.g., Cruz et al., 2017; Fairchild et al., 2001; Lewis et al., 2011; Roberts et al., 1998; Steponaitis et al., 2015). Trace element to calcium ratios can track PCP and/or water–rock interactions, which change based on soil and water conditions in the local environment (e.g., Cruz et al., 2017; Fairchild et al., 2000, 2001; Sinclair et al., 2012). In drier conditions, water moves more slowly through the karst above a cave, so it has more time to degas and become saturated with calcite (Tremaine & Froelich, 2013). During PCP, Mg and Sr are preferentially excluded from the calcite crystal lattice, so Mg/Ca and Sr/Ca ratios in groundwater increase (Fairchild et al., 2000). Non-PCP interactions between water and host rock, also called calcite recrystallization, can also occur in the karst, especially when water residence time is high during dry periods. The chemical signature of recrystallization is similar to that of PCP, but with a different relationship between Mg/Ca and Sr/Ca (Sinclair et al., 2012). Therefore, Mg/Ca and Sr/Ca in stalagmites provide an estimate of aquifer recharge and water availability that can serve as an independent hydroclimate proxy, providing a method to examine whether stalagmite $\delta^{18}O$ primarily reflects changes in local moisture availability (Tremaine & Froelich, 2013).

2. Methods

2.1. Regional Setting and Cave System

We collected the stalagmite outside the city of Playa del Carmen, Quintana Roo, in the northeast YP (20°35.244′N, 87°8.042′W, 10–20 m above sea level) (Figure 1a). The RS cave entrance is about 5 km from the Caribbean coast. Temperature and relative humidity in RS have been monitored ~continuously since 2014. Annual mean temperature in the collection chamber varied by 0.1°C, from 24.6°C to 24.7°C (Lases-Hernandez et al., 2019; Medina-Elizalde, Polanco-Martínez, et al., 2016). The steady temperature limits the effect of calcification temperature on stalagmite $\delta^{18}O$ ($\delta^{18}O_{calcite}$). RS has a relative humidity of 99.6% ± 0.9% throughout the year (Lases-Hernandez et al., 2019; Medina-Elizalde, Polanco-Martínez, et al., 2016).

Three years of drip water $\delta^{18}O$ ($\delta^{18}O_{drip}$) monitoring at 16 drip sites indicated that $\delta^{18}O_{drip}$ reflects the $\delta^{18}O$ composition of precipitation ($\delta^{18}O_{precip}$) and that evaporation does not influence $\delta^{18}O_{drip}$ (Lases-Hernandez

Table 1
U-Series Data for 16 Samples From RS1 Based on Analyses at MIT Between 2015 and 2018

Sample ID	Depth (mm)	^{238}U (ng/g)	$\pm 2\sigma$	^{232}Th (pg/g)	$\pm 2\sigma$	$d^{234}U$ (‰)	$\pm 2\sigma$	$(^{230}Th/^{238}U)$ activity	$\pm 2\sigma$	$^{230}Th/^{232}Th$ ppm atomic	$\pm 2\sigma$
RS1-G1	63	170	3.4	1,225	24.7	−5	2	4.95E−02	5.30E−04	109	1.2
RS1-A1	133	147	2.9	269	5.6	−2	2	4.84E−02	5.99E−04	421	4.0
RS1-A2	133	142	2.8	606	12.4	−8	2	4.95E−02	5.93E−04	184	1.6
RS1-3*	259	119	2.0	369	8.0	−3	3	5.16E−02	7.00E−04	264	5
RS1-4*	328	134	3.0	571	12.0	−5	7	5.93E−02	8.00E−04	220	3
B145	343	171	3.4	229	4.6	−5	1	4.95E−02	4.13E−04	587	5.1
RS1-B1	426	154	3.1	153	3.3	−6	2	4.96E−02	5.55E−04	795	8.3
RS1-B2	426	158	3.2	16	1.2	−9	2	4.89E−02	5.49E−04	7,475	547
RS1-G2	508	142	2.8	124	3.1	−4	1	5.00E−02	7.84E−04	913	20
RS1-G3	574	156	3.1	69	2.6	−7	1	5.12E−02	5.35E−04	1,837	61
C100	684	139	2.8	148	3.2	−5	2	5.13E−02	5.36E−04	764	10
RS1-G4	749	134	2.7	290	6.3	−4	2	5.20E−02	5.29E−04	380	4.9
RS1-3	791	160	3.2	223	15.9	−4.3	1.6	5.25E−02	7.48E−04	598	41.8
RS1-C1	895	147	2.9	549	11.0	22	2	5.35E−02	5.52E−04	227	1.2
RS1-C2	895	135	2.7	171	3.6	−4	2	5.80E−02	7.46E−04	726	7.8
RS1-4	927	110	2	53.1	16.9	1	2	5.37E−02	1.20E−03	1,762	561

et al., 2019). The average $\delta^{18}O_{drip}$ is −3.9‰ ± 1‰ (± 2SD; n = 1,043 drip samples collected over 3 years throughout the RS cave system; each sample represents drip water collected for ~48 h), and the amount-weighted $\delta^{18}O_{precip}$ is −3.7‰ (n = 36 monthly rainfall samples) (Lases-Hernandez et al., 2019). Therefore, the cave drip water accurately records regional $\delta^{18}O_{precip}$ within typical variability. Although the permeable vadose zone is thin (~10 m), rainfall infiltration rates vary within the cave, with some drip sites showing increased discharge immediately after rainfall events and others lagging by up to 3 months (Lases-Hernandez et al., 2019).

Modern drip water analyses also showed that Mg/Ca and Sr/Ca decreased significantly during the transition from a dry hydrological year (only 53% of historical mean annual precipitation) to the wettest period studied with >1,500 mm in 1 year (Lases-Hernandez, 2020). Furthermore, farmed calcite analyses indicate that there is active PCP occurring in RS (Lases-Hernandez, 2020). In farmed calcite grown over approximately 2 years, there are positive correlations between Mg/Ca and stable isotope data but no significant correlation between Sr/Ca and stable isotope ratios (Lases-Hernandez, 2020); however, Lases-Hernandez (2020) argues that the lack of correlation with Sr/Ca could be due to the limited variations in precipitation amounts captured in farmed calcite; there was no farmed calcite experiment during the driest hydrological year in 2016.

Drip water samples closest to the RS1 collection site (Drip Station A) show muted ~2‰ intra-annual (seasonal) variability in $\delta^{18}O$ (Lases-Hernandez et al., 2019) and annual mean $\delta^{18}O_{drip}$ similar to the amount-weighted annual mean $\delta^{18}O_{precip}$, which suggests that this chamber has a large reservoir with a mixture of seasonal and seepage flow that averages approximately 1 year of rainfall accumulation (Lases-Hernandez et al., 2019); most recently, the water residence time was estimated to be 4–15 months (Lases-Hernandez, 2020). Therefore, this study focuses on variability at annual or greater scales. The stalagmite was sampled for proxies with the aim of producing ~annual resolution data. Therefore, we do not expect to resolve individual tropical cyclone events in the record.

2.2. U–Th Dating, Age Modeling, and Microstratigraphy

The age model for RS1 is constrained by U–Th dating of 16 horizons distributed throughout the length of the stalagmite, performed at MIT, and including replicates (Tables 1 and 2; Figure 2). Dating samples weighing

Table 2
U-Series Dates (n = 16) Calculated Based on Data in Table 1

Sample ID	Depth (mm)	Uncorr. age (years)	±2σ	Corr. age (years before chem.)	±2σ	d^{234}U init. (‰)	±2σ	Corr. age (years before 1950)	±2σ	Excl.	Repl.
RS1-G1	63	5,564	62	5,345	126	−4.8	1.8	5,280	126		
RS1-A1	133	5,423	69	5,368	29	−1.8	1.8	5,300	70		Y
RS1-A2	133	5,581	69	5,451	66	−8.1	1.7	5,390	69		Y
RS1-3*	259	5,800	90	5,710	100	−3.0	3.0	5,640	100	Y	
RS1-4*	328	6,700	100	6,570	120	−5.0	7.0	6,500	120	Y	
B145	343	5,560	48	5,520	52	−5.1	1.0	5,450	52		
RS1-B1	426	5,578	65	5,548	66	−6.1	1.6	5,480	66		Y
RS1-B2	426	5,517	64	5,514	10	−8.7	1.7	5,450	64		Y
RS1-G2	508	5,611	91	5,584	92	−3.8	1.3	5,520	92		
RS1-G3	574	5,775	63	5,761	63	−7.6	1.4	5,690	63		
C100	684	5,772	63	5,740	65	−4.8	1.5	5,670	65		
RS1-G4	749	5,844	62	5,778	70	−4.3	1.8	5,710	70		
RS1-3	791	5,912	87	5,870	23	−4.4	1.6	5,806	87		
RS1-C1	895	5,867	63	5,756	62.9	22.0	1.7	5,690	63	Y	Y
RS1-C2	895	6,541	88	6,503	89.7	−4.2	1.8	6,440	90	Y	Y
RS1-4	927	6,013	139	5,998	15	0.9	2.1	5,934	139	Y	

Note. Ages are given as corrected (corr.) and uncorrected (uncorr.); corrected age in years before present (where present is 1950) was used for age–depth modeling. Dates that were excluded (excl.) or were replicates that were averaged to one date (repl.) are noted in the final two columns. Calculated with an initial ^{230}Th/^{232}Th atomic ratio of $4.4 \pm 2.2 \times 10^{-6}$.

~150 mg were drilled with a vertical mill. Powders were dissolved and spiked with a ^{229}Th–^{233}U–^{236}U tracer. Based on methods detailed in Edwards et al. (1987), U and Th were isolated using coprecipitation with Fe oxyhydroxides and eluted using columns with AG1-X8 resin. A total procedural blank was included with each set of dating samples. U and Th fractions were measured on a Nu Plasma II-ES MC-ICP-MS, as described in Burns et al. (2016). We used an initial ^{230}Th/^{232}Th atomic ratio of $4.4 \pm 2.2 \times 10^{-6}$ to correct for initial ^{230}Th (Taylor & McLennan, 1985). Other initial ratios were also tested but were not used because they did not change the stratigraphic order of the dates. All ages are reported as years before present (yr BP), where present is 1950 (Table 2).

Close to the bottom of the stalagmite (794 mm from the top), we observed a ~50 mm-long dark brown region (Figure 1). There were no visible layers within the darker region, suggesting that the layering was dissolved and recrystallized, so we infer that this dark area is a diagenetically altered segment. The top of the dark region was used as the cutoff for all analyses, so the dark portion and layers below were not included in this study. Visual inspection also revealed a potential hiatus near the top of the sample (Figure 1f). Therefore, the region above the deposited dark material (the top 23 mm) was also excluded from climate analysis or age–depth calculations.

Six of the 16 total dates were not included in the final age model due to low reproducibility, location outside hiatuses, or proximity to possible dissolution features (Table 2; supporting information). Replicates from the same depth were discarded if they did not overlap within 2SD, and samples within 10 mm of a possible dissolution feature were not included.

Age–depth relationships were calculated with the COPRA program (Breitenbach et al., 2012) in MATLAB (version R2018b). The age–depth model was based on the median of 2000 Monte Carlo simulations of eight unique U–Th dates (10 including replicates). We calculated an error-weighted mean age and 2SD error for replicate ages from depth = 133 and 426 mm using IsoplotR. The weighted results were 5,346 ± 49 and 5,465 ± 46 yr BP; these weighted ages and errors were used as inputs for the U–Th age model. We
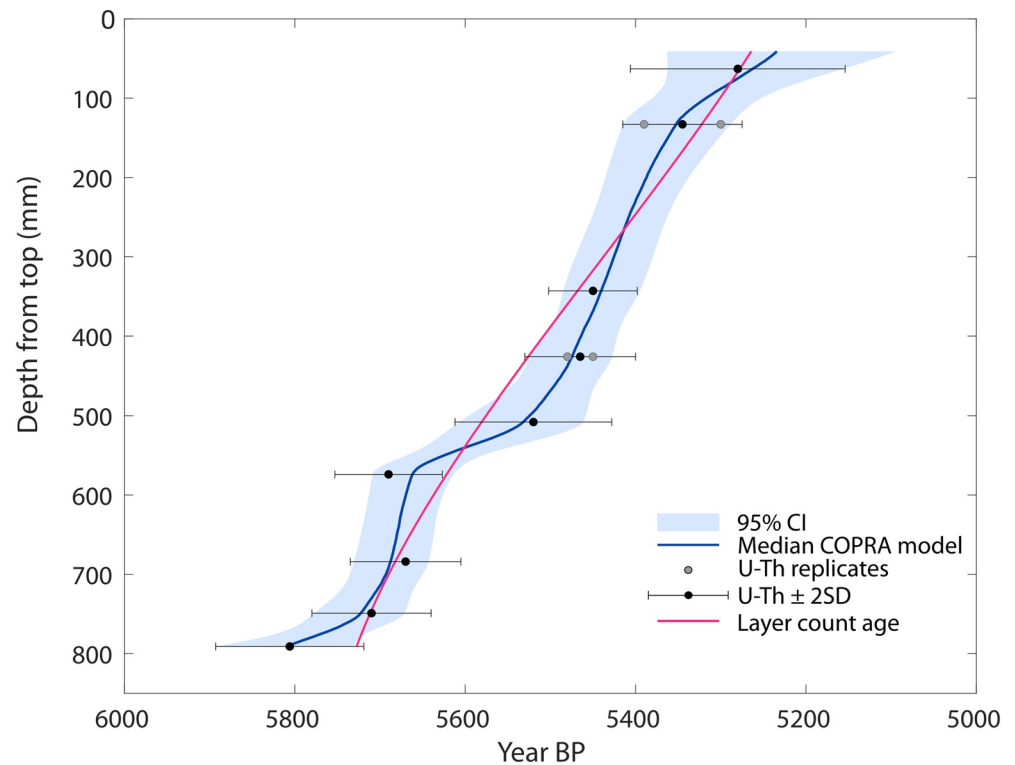
Figure 2. Age–depth relationship for RS1 based on Monte Carlo modeling of 10 U–Th dates and layer counting. The median and 95% confidence interval age models used U–Th dates only; the layer count-enabled model is shown in pink and is used for the time series plots in subsequent figures.

calculated upper and lower bounds of the 95% confidence interval (CI) to accurately report the uncertainty of the age–depth model. The median age model and the 95% CI limits all fall within the 2SD uncertainty of each U–Th date. The oldest part of the stalagmite used in this study was dated to 5,809 ± 52 yr BP and the youngest was 5,234 ± 130 yr BP. Therefore, based on U–Th results, the useable portion of the stalagmite spans 575 ± 91 years.

RS1 shows a high deposition rate with visually distinct ∼2-mm-thick layers throughout the stalagmite, likely reflecting annual deposition (Figure 1). The layers were distinct enough to count and measure in photographs or hand sample, allowing for counting without microscopy or thin sections. We performed visual counts of the same vertical extent, which yielded 463 ± 38 layers (mean ± 2SD of multiple counts by GSM and GC). The U–Th age and layer count overlapped within uncertainty, so we established a layer count-enabled age–depth model.

We used two U–Th dates (one from the top and one from the bottom) as markers of absolute age: working from the top anchor date, we counted layers upward to reach the top of the stalagmite (stopping at the hiatus) then went back to the anchor and counted layers downward between other U–Th data points to measure relative change in age. We repeated this process with the lower anchor, counting downward to the bottom (stopping at the dark excluded area) then upward between each U–Th date. There was a 2-year discrepancy between the counted age from the top versus bottom anchors, so we averaged them to make the counted model. We used the date second from the bottom as an anchor (instead of the date closest to the bottom) because of a major shift in growth rate based on U–Th age–depth modeling that was not replicated in the stalagmite layer counting. Using the counted model, we generated a simplified age–depth model based on a cubic function ($r^2 > 0.99$; Figure 2) which was used to calculate ages for the time series of geochemical proxies. All age uncertainties reported in this study are based on the 95% CI of the U–Th age model. For a demonstration of how the oxygen isotope record varies when plotted on the layer count-enabled age model versus the median age–depth model from U–Th ages only, see supporting information.

2.3. Proxy Measurements ($\delta^{18}O$ and $\delta^{13}C$; Mg/Ca and Sr/Ca)

Calcite samples for stable isotope analysis were drilled at a ~2-mm resolution in a continuous track parallel to the growth axis ($n = 335$ samples). The $\delta^{18}O$ and $\delta^{13}C$ analyses were carried out using a Thermo Scientific MAT253 Stable Isotope Ratio Mass Spectrometer online coupled to a Kiel IV at University of California Santa Barbara. About 40–50 µg of each sample were reacted using 105% phosphoric acid addition. The evolving CO_2 was cryogenically cleaned before introduction into the mass spectrometer. The $\delta^{18}O$ and $\delta^{13}C$ data are reported on the Pee Dee Belemnite scale. The precision of the $\delta^{18}O$ and $\delta^{13}C$ analysis, assessed by analyzing NBS 19 standards, was ±0.07‰ and ±0.05‰ (2SE), respectively.

Additional samples (weight = ~2 mg) were drilled for trace element analysis at a ~2-mm resolution in locations within 0.25 mm of the stable isotope powder samples; for any difference larger than 0.25 mm, the two types of data are reported at separate depths. Each sample was dissolved and diluted with 3% nitric acid. Standards with similar Mg/Ca and Sr/Ca ratios and concentrations were prepared using single-element standards. Analyses of Mg, Sr, and Ca were performed at MIT on an Agilent 7900 ICP-MS in no-gas mode. Data were corrected for blank intensities, isotopic abundances, and instrumental drift. Relative deviation in standards during 1 day of analysis averaged 4% ($n = 5$ standards per day) after these corrections. Replicate runs of identical solutions on different days also varied by an average of 4%. Replicate powders drilled from the same depth but at different distances from the growth axis varied by 1% or less in both Mg/Ca and Sr/Ca. All future references to trace elemental ratios in this work will be referring to Mg/Ca and Sr/Ca.

2.4. Data Analysis

We used Spearman's rank correlation, a nonparametric correlation analysis, to test for relationships between the proxies. We used a two-tailed correlation; p-values < 0.05 were considered significant. The rationale behind using Spearman's rank correlation instead of a parametric correlation analysis, like Pearson's correlation coefficient, was to remove the assumption of a linear relationship between the proxies. Instead, Spearman's ρ measures monotonic relationships. A monotonic relationship is more likely than a linear relationship between geochemical proxies controlled by different physical mechanisms, even if they are all controlled (at a high level) by hydroclimate; in other words, we expect both $\delta^{18}O$ and Mg/Ca to increase with drying, but we do not expect Mg/Ca to increase linearly with $\delta^{18}O$. We also used a wavelet toolbox (Grinsted et al., 2004) with MATLAB versions 2018b and 2020a for wavelet analyses of periodicity (supporting information).

3. Results

3.1. U–Th Dating and Age Model Development

This stalagmite has precise age control, with age model uncertainty substantially lower than those found in nearby stalagmites of similar age due to its low detrital Th content (e.g., Akers et al., 2016; Pollock et al., 2016; Winter et al., 2020, Table 1); the median 2SD age uncertainty of U–Th dates was ±70 years. Therefore, RS1 and Itzamna are the oldest stalagmite records from the YP with median age uncertainty <100 years (Medina-Elizalde et al., 2017).

After establishing the layer count-enabled age–depth model, we found that the useable portion of the stalagmite with sampling coverage grew from 5,721 ± 52 to 5,265 ± 130 yr BP, or 456 years (2SD uncertainty based on U–Th dates).

3.2. Stable Isotopes

3.2.1. Comparison to Modern Drip Water

We sampled RS1 continuously at 2-mm resolution ($n = 335$ samples) in a region of the speleothem modeled to span 456 years, meaning that each sample averaged ~1.3 years; all proxy data were resampled to annual resolution ($n = 457$ points) to remove potential effects of sampling frequency and variable growth rate. Mean $\delta^{18}O_{calcite}$ was −5.50‰ ± 1.02‰ and mean $\delta^{13}C_{calcite}$ was −9.43‰ ± 1.99‰ (mean ± 2SD; see supporting information for statistics without resampling).

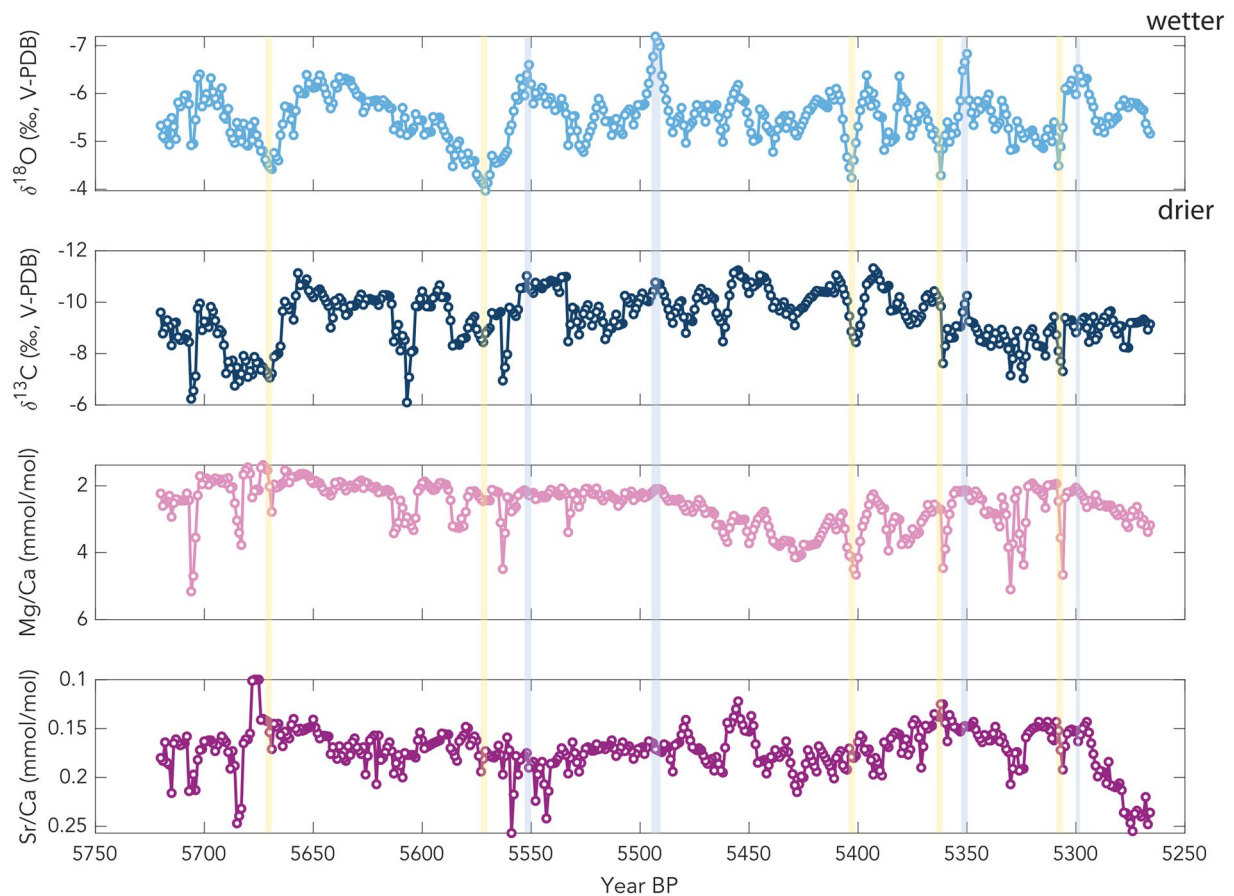**Figure 3.** $\delta^{18}O$, $\delta^{13}C$, Mg/Ca, and Sr/Ca data for the growth period of RS1, a stalagmite from the Yucatán Peninsula, resampled to annual resolution. Vertical bars highlight periods with $\delta^{18}O$ values at least 2SD greater than (tan) or less than (blue) the mean (−5.50‰). See supporting information for a version of this figure without resampling.

Mean $\delta^{18}O_{drip}$ in the modern RS cave system is $−3.9‰ \pm 1‰$ (VSMOW; ± 2SD). Using the Tremaine et al. (2011) equation for equilibrium fractionation and temperature = 24.5°C, we calculate that equilibrium precipitation of calcite would yield $\delta^{18}O_{calcite} = −4.8‰$. This value overlaps with $\delta^{18}O_{calcite}$ in the late Holocene stalagmite from RS (Itzamna $\delta^{18}O_{calcite} = −4.8‰ \pm 0.1‰$; mean ± 2SE) within error, suggesting late Holocene precipitation at or near equilibrium.

For a back of the envelope calculation of potential drip water composition in the mid-Holocene, we assume mean cave air temperature was still 24.5°C. The reversed Tremaine et al. (2011) equilibrium calculation, using $\delta^{18}O_{calcite} = −5.5‰$, suggests $\delta^{18}O_{drip}$ would have been approximately −4.6‰. This more negative value (in comparison to modern drip water, −3.9‰) supports previous research showing that the mid-Holocene was wetter than the late Holocene, as detailed in the Section 4.

3.2.2. Time Series Analysis

$\delta^{18}O_{calcite}$ and $\delta^{13}C_{calcite}$ are significantly positively correlated with each other in the RS1 growth period (Figures 4 and 5; $\rho = 0.507$, p-value << 0.001); furthermore, when the record is broken into 50-year-long windows, they are significantly correlated in eight out of nine windows. Although some research has linked covariation in $\delta^{18}O$ and $\delta^{13}C$ to kinetic fractionation (e.g., Lachniet et al., 2004), previous work in this cave found that kinetic fractionation was not significant and that relative humidity is near 100% throughout the year (Lases-Hernandez et al., 2019; Medina-Elizalde, Burns, et al., 2016); therefore, we suggest that the correlation between $\delta^{18}O_{calcite}$ and $\delta^{13}C_{calcite}$ is due to their common dependence on hydrologic variability.

There were four short periods with $\delta^{18}O$ ratios 2SD less than the mean, interpreted as wet periods that ended at $5,551 \pm 43$, $5,493 \pm 36$, $5,351 \pm 41$, and $5,299 \pm 55$ yr BP (Figure 3). There were also five similarly
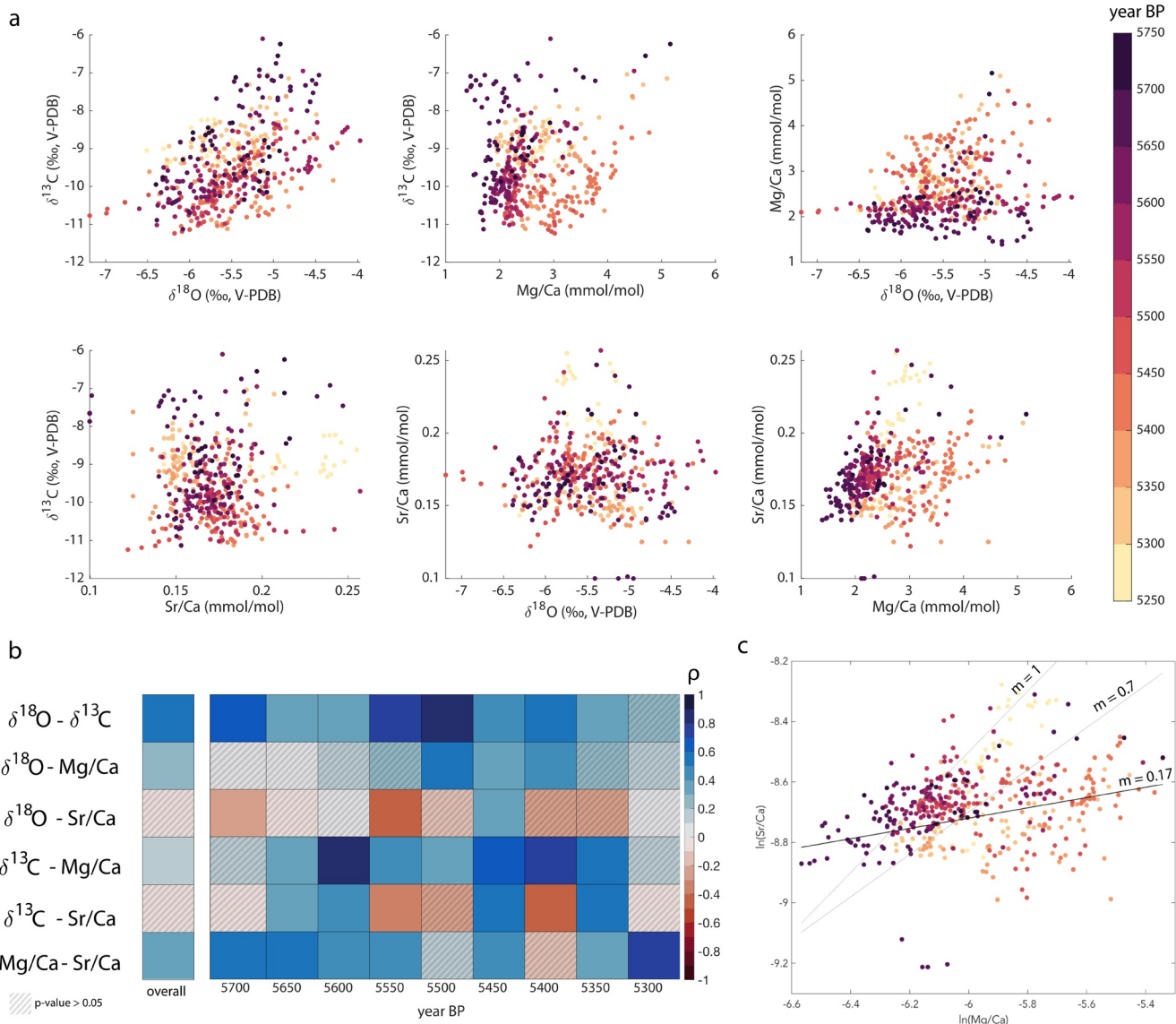
Figure 4. (a) Crossplots of trace element to calcium ratios and stable isotope data measured in RS1. All data have been resampled to annual resolution to remove sampling bias and are colored according to their age. (b) Correlation coefficient (ρ) for Spearman's rank correlation tests on 50-year-long windows and overall. Cross hatching shows p-value > 0.05, which is not significant. (c) Crossplot of Sr/Ca and Mg/Ca ratios; points are colored according to the colorbar in a. The RS1 data have a nearly flat slope ($m = 0.17$). Higher slopes ($m = 0.7–1$) associated with prior calcite precipitation (Sinclair et al., 2012) are shown for reference but do not match the RS1 data.

short periods with δ^{18}O at least 2SD greater than the mean, interpreted as dry periods, ending at 5,668 ± 64, 5,571 ± 63, 5,404 ± 39, 5,363 ± 39, and 5,308 ± 49 yr BP (Figure 3). Note that absolute age is based on the layer count-enabled age model and the 2SD age uncertainty is based on the U–Th age model. During both wetter and drier events, δ^{18}O values >2SD outside the mean (interpreted as the culmination of the event) lasted for less than 10 years but were part of a longer period of change (decades long).

3.3. Trace Elements

Our results show that mean mid-Holocene Mg/Ca was 2.61 ± 1.29 mmol/mol and Sr/Ca was 0.17 ± 0.05 mmol/mol (± 2SD). Spearman's rank correlations showed a weak but significant correlation between annual Mg/Ca and Sr/Ca data ($\rho = 0.35$, p-value << 0.01; Figure 4), meaning that Mg and Sr share some common controls. The youngest 50 years (5,300–5,250 yr BP) have the highest correlation ($\rho = 0.76$,
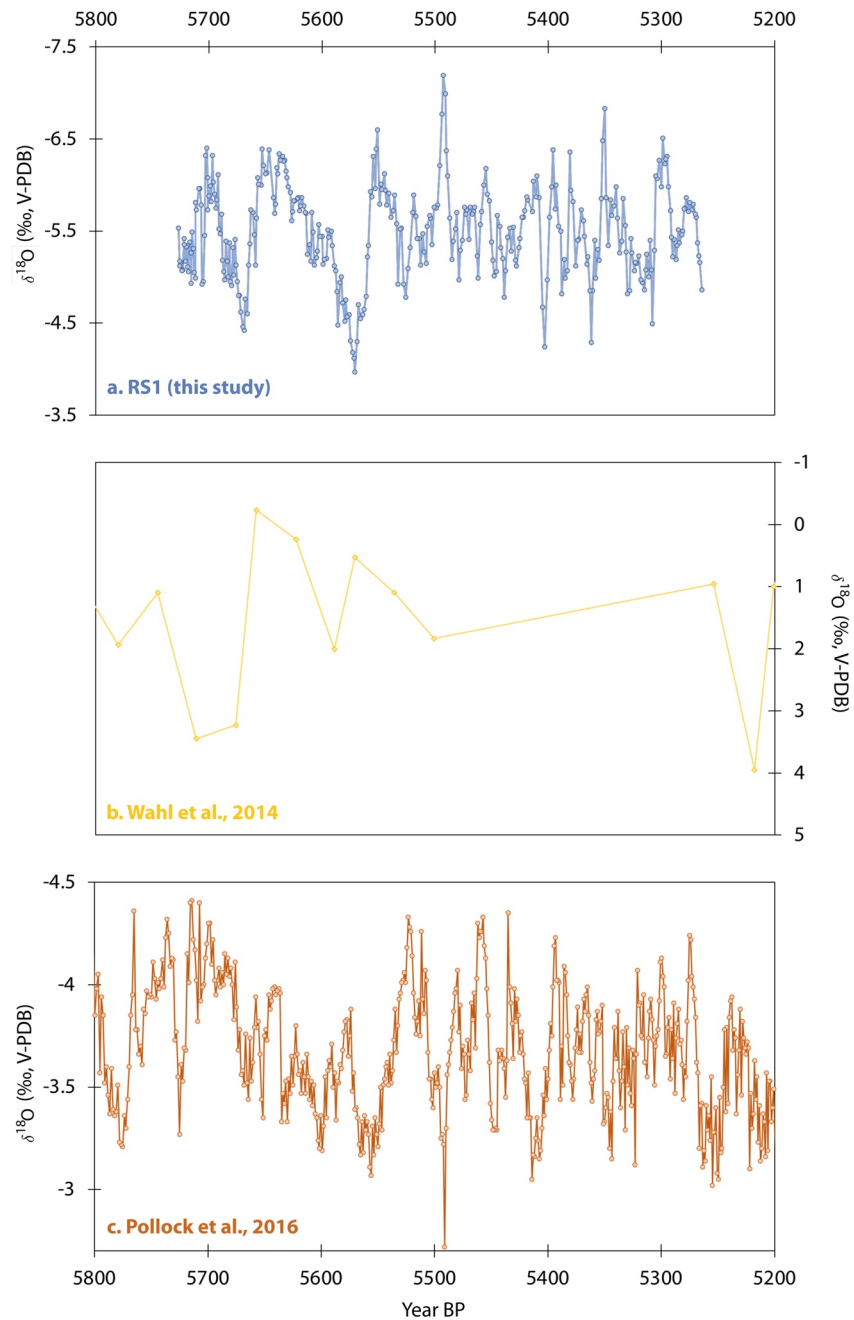
Figure 5. Oxygen isotope ratio data for RS1 (this study, a), a sediment core from Lago Puerto Arturo (Wahl et al., 2014; b), and Chen Ha, a speleothem from Belize (Pollock et al., 2016; c). Data are plotted without resampling or smoothing.

p-value << 0.01), perhaps because Mg/Ca and Sr/Ca both increase during that period (at the same time as a short increase in $\delta^{18}O$), interpreted as drying. It is possible that this period was the beginning of a severe dry event that produced the hiatus that ended the RS1 record.

We tested whether the relatively low ρ value for the correlation between Mg/Ca and Sr/Ca was due to sub-decadal noise by applying a low-pass Butterworth filter at 2-year and 5-year frequencies. The correlation only increased a small amount ($\rho = 0.36$ for 2-year low-pass and $\rho = 0.37$ for 5-year low-pass); the minimal increase in rank correlation indicates that subdecadal noise was not the primary difference between Mg/Ca

and Sr/Ca. Given these results, we hypothesize that Sr/Ca did respond to hydroclimate changes, but Sr incorporation was additionally influenced by growth rate and axis changes.

There is low but significant correlation between Mg/Ca and $\delta^{18}O_{calcite}$ ($\rho = 0.25$, p-value $<< 0.01$) and $\delta^{13}C$ ($\rho = 0.10$, p-value $= 0.027$) throughout the record (Figure 4). Correlations between Sr/Ca and stable isotope data were not significant, yielding $|\rho| < 0.06$ and p-value > 0.3 for both $\delta^{18}O$ and $\delta^{13}C$ (Figure 4).

We also tested correlations within 50-year-long windows, rather than in the full record, to allow for changes in the initial trace element composition of drip water through time. Within these windows, Sr/Ca and Mg/Ca are more correlated with $\delta^{13}C$ than they are with $\delta^{18}O$: trace element ratios and $\delta^{13}C$ are significantly positively correlated in more windows (Sr/Ca = 4/9, Mg/Ca = 7/9) than trace elements and $\delta^{18}O$ (Sr/Ca = 1/9, Mg/Ca = 3/9) (Figure 4).

That said, there are also several instances where Mg/Ca and Sr/Ca values increase dramatically, sometimes as much as twofold. Many of the increases in trace element ratio values coincide with elevated stable isotope values (indicating drier conditions), despite a weaker Sr/Ca response (Figures 3 and 4). More specifically, increases in Mg/Ca occur synchronously with previously noted $\delta^{18}O$ excursions at 5,668 ± 64, 5,404 ± 39, 5,363 ± 39, and 5,308 ± 49 yr BP. This result, along with significant correlations between Mg/Ca, $\delta^{13}C$, and $\delta^{18}O$, supports the interpretation of $\delta^{18}O$ as a proxy for local moisture availability.

However, we also note periods where $\delta^{18}O$ and the other three proxies diverge. One example occurs at 5,571 ± 63 yr BP, where $\delta^{13}C$, Sr/Ca, and Mg/Ca all increase rapidly a few years after an increase in $\delta^{18}O$ (Figure 3, noted with tan bar); the trace element and $\delta^{13}C$ values lag behind the $\delta^{18}O$ values. These anomalies could be related to threshold behavior in the epikarst, meaning that increases in PCP, water–rock interactions, and degassing, and therefore increases in Sr/Ca, Mg/Ca, and $\delta^{13}C$, happen more slowly than the $\delta^{18}O_{precip}$ signal is transmitted to the stalagmite.

As indicated above, Sr/Ca behaves differently from Mg/Ca during several events in the RS1 record; these events are one source of low correlation between Sr/Ca and other proxies. For example, during the dry anomaly centered at 5,404 ± 39 yr BP (Section 3.2.2), there is a synchronous increase in $\delta^{18}O$, $\delta^{13}C$, and Mg/Ca ratios but not Sr/Ca (Figure 3). Increased proxy values suggest a 20-year-long period with drier hydroclimate, which we report with high confidence because of the significant correlations and similar event duration between three of the four proxies (Figure 3). During the 50-year-long window encompassing that event, there are significant positive correlations between $\delta^{18}O$, $\delta^{13}C$, and Mg/Ca but not with Sr/Ca; in fact, there is a significant negative correlation between $\delta^{13}C$ and Sr/Ca (Figure 4b).

Furthermore, when Sr/Ca was measured in modern farmed calcite and drip water from RS, results indicated that Sr/Ca was not correlated with precipitation amount on monthly time scales (Lases-Hernandez, 2020). The lack of correlation was ascribed to a lack of major differences in precipitation amount during the calcite growth. In combination with the calcite results reported here, it appears that there are additional factors controlling Sr/Ca in RS. These primary drivers could include sea spray and calcite growth rate changes; previous research in RS demonstrated that the drip water was enriched in chloride in comparison to rainfall (Lases-Hernandez, 2020).

3.3.1. Relationship With Drip Water Trace Element Compositions

Regression of the calcite Mg/Ca and Sr/Ca data in log space yielded a nearly flat slope ($m = 0.17$; Figure 4c). This result suggests that PCP was not the dominant control on Mg/Ca and Sr/Ca during the mid-Holocene (Sinclair et al., 2012). Instead, the regression yields a slope similar to that reported to relate to water–rock interactions ($m = 0.18$), including calcite recrystallization (Sinclair et al., 2012). Therefore, calcite recrystallization could be the main driver of variability in Mg/Ca and Sr/Ca ratios (Sinclair et al., 2012). During the last part of the record (from 5,300 yr BP to the hiatus), the data have a different slope ($m = 1.11$, $n < 40$ samples), which could indicate PCP leading into the hiatus at the top of the sample.

Lases-Hernandez (2020) reports that there is active PCP in the modern cave. Therefore, the lack of evidence for PCP in trace element ratios from RS1, when considered alongside stable isotope data that suggest a wetter hydroclimate during the mid-Holocene, supports increased precipitation in comparison to the late Holocene and today. We cannot definitively confirm whether there was PCP in the preindustrial late Holocene, however, without trace element ratios from a late Holocene stalagmite. Therefore, Mg/Ca may provide an
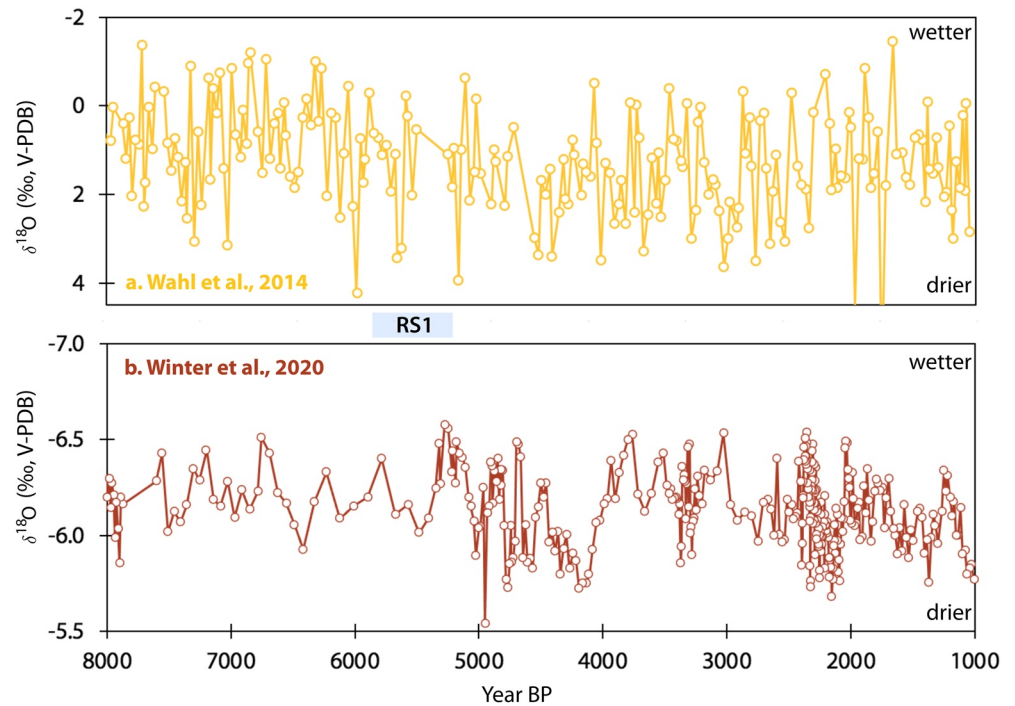
Figure 6. Longer records from Guatemala covering the mid-Holocene and late Holocene. (a) A sediment core from Lago Puerto Arturo (Wahl et al., 2014) and (b) a speleothem from Grutas de Rey Marcos (Winter et al., 2020). The blue box indicates the growth period of RS1 (this study).

independent tool to assess whether the stable isotope data primarily reflect hydrological changes in RS, but Mg/Ca needs to be more broadly applied to be most useful.

3.4. Spectral Analysis

We used wavelet analysis to quantitatively examine periodicity (supporting information). The limited window captured by the stalagmite means that it is difficult to find long-term periodicity that is statistically significant, but the proxies recorded signals with 32–128 year periods with limited statistical significance (supporting information). Due to the lack of robust periods, we will focus on other types of comparisons.

3.5. Comparison to Other Records

There are several existing paleoclimate records from the YP region (see Section 1 for a longer summary), including both sediment and speleothem records. Here, we compare RS1 to three such records: Lago Puerto Arturo (LPA) from Wahl et al. (2014), which used stable isotope ratios as proxies for hydroclimate; Chen Ha from Pollock et al. (2016), a stalagmite with a similar resolution covering a similar time period (Figure 5); and GU-RM1, a speleothem from Grutas del Rey Marcos, Guatemala in Winter et al. (2020), which provides longer context for RS1. The LPA core and GU-RM1 speleothem each have a much lower resolution than RS1 or Chen Ha, with only nine data points from LPA and eight from GU-RM1 during the RS1 growth period (Figures 5 and 6).

Qualitatively, however, the RS1 and LPA δ^{18}O records have a very similar pattern, with an increase toward wetter conditions around 5,675–5,650 yr BP, followed by a shift back to drier conditions after 5,600 yr BP. RS1 appears to be a higher resolution version of the Wahl et al. (2014) record from the beginning of RS1 to 5,550 yr BP (Figure 5).

Pollock et al. (2016) does not show the same change toward wetter conditions around 5,675 and has a different or lagged pattern than the other two records from 5,700 to 5,500 yr BP (Figure 5); for example, the maximum δ^{18}O value in RS1 occurs at 5,571 yr BP, and the Chen Ha sample has a similarly shaped local maximum at 5,556 yr BP. A lead or lag of ~25 years would be within age model uncertainty for both Pollock et al. (2016) and RS1.
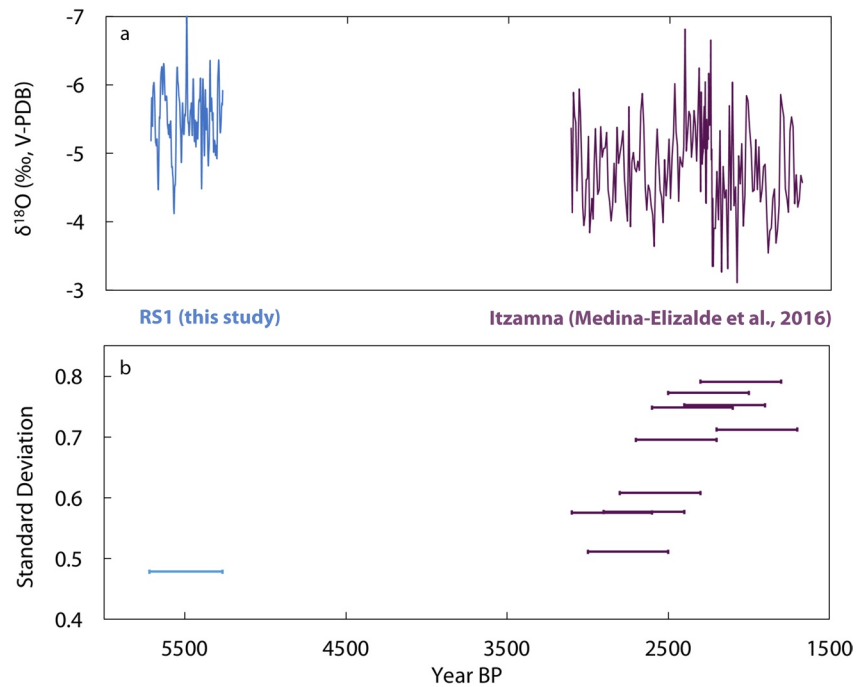
Figure 7. (a) Time series records of $\delta^{18}O_{calcite}$ in Itzamna (Medina-Elizalde, Burns, et al., 2016) and RS1. (b) Standard deviation of 500-year-long snapshots of $\delta^{18}O_{calcite}$ from Itzamna (Medina-Elizalde, Burns, et al., 2016) and RS1 (with an 8-year low-pass Butterworth filter). Variability and median $\delta^{18}O$ are both significantly lower in RS1 than in Itzamna (*F* test for variance, *p*-value << 0.001; Mann–Whitney *U* test for median, *p*-value << 0.001).

In context with longer YP records, such as those of Wahl et al. (2014) and Winter et al. (2020) from Guatemala, RS1 grew at the end of what previous studies have called the wetter mid-Holocene or stable regime (Figure 6). We compared RS1 to these two data sets because they each encompass the full length of RS1, plus several thousand years before and after its growth. RS1 stopped growing at 5,234 ± 130 yr BP, just as a centennial-scale drying period began in the Winter et al. (2020) speleothem (Figure 6).

Itzamna, a stalagmite from RS that grew during a more recent time period than RS1 (∼3,000–1,500 yr BP), has been used to study the Maya Terminal Classic Period. Because these two stalagmites came from the same cave and have similar dating errors, comparing them allows for an analysis of precipitation variability and amount over time. The late Holocene Itzamna $\delta^{18}O$ record has a lower resolution, with an average of 8 years per sample, so we applied an 8-year low-pass Butterworth filter to the higher resolution RS1 $\delta^{18}O$ record. This filtering method served to remove any variance that would not have been captured in the Itzamna record.

The median $\delta^{18}O_{calcite}$ for Itzamna was −4.9‰, significantly less negative than RS1's median $\delta^{18}O_{calcite} = -5.5‰$ (Figure 7; Mann–Whitney *U* test, *p*-value << 0.001). The variance in the two stalagmites is also statistically different (*F* test, *p-value* << 0.001), with RS1 showing less variability than Itzamna (Figure 7); variability in Itzamna increased over time but was always greater than that in RS1. We acknowledge that there may be differences in how $\delta^{18}O$ responded to precipitation change in the two stalagmites and that these results are not purely indicative of climatic shifts. Nonetheless, comparing samples from the same cave controls for regional or local climate features that could interfere with comparing stalagmites from different caves.

4. Discussion

4.1. Mid-Holocene Hydrological Variability in the RS1 Record

There are notable dry periods (more positive ratios, >2SD above mean $\delta^{18}O_{calcite}$) reaching local $\delta^{18}O$ maxima at 5,668 ± 64 and 5,571 ± 63 yr BP that lasted for 20–50+ years. We note that some Mesoamerican droughts

in both the Common Era and the past century had similar multidecadal lengths (e.g., Medina-Elizalde, Burns, et al., 2016). This similarity shows that multidecadal precipitation cycles are an integral feature of YP hydroclimate, occurring even during a period of inferred higher mean precipitation and reduced precipitation variance. Both of the multidecadal dry periods have a sawtooth pattern in the $\delta^{18}O_{calcite}$, with slow drying and a rapid change back to wetter conditions. Although the $\delta^{18}O_{calcite}$ was only outside the 2SD envelope briefly (a few years at the inferred maximum of the dry period), the slow drying lasted for decades.

The RS1 record also revealed three shorter dry intervals (duration ≤ 20 years) at 5,404 ± 39, 5,363 ± 39, and 5,308 ± 49 yr BP, noted as anomalies in both stable isotope and Mg/Ca data, which were previously undetected in lower resolution records (e.g., Wahl et al., 2014). In addition, although wet intervals are less well studied than droughts in the YP, we also found a ~20-year-long event with a local $\delta^{18}O$ minimum at 5,493 ± 36 yr BP. These short events were only detected because of the ~annual sampling resolution of RS1.

Taken together, the qualitative agreement and the statistical correlations between trace elements and stable isotopes show that it is feasible to use $\delta^{18}O$, $\delta^{13}C$, and Mg/Ca as paleoclimate proxies in this region on multiyear time scales. Furthermore, we suggest that it is prudent to collect data on multiple types of proxies because they record hydrological variability in different ways, potentially enriching the interpretation of the record.

4.2. Comparison to Other Records

Analysis of RS1 compared to Itzamna showed decreased variability and increased mean $\delta^{18}O$ in the mid-Holocene compared to the late Holocene. Although it would be ideal to have one stalagmite sample that grew over the entire mid-Holocene and late Holocene, we do not have that specimen. Instead, we have to assume that the differences in the variability of both $\delta^{18}O$ records are primarily due to changes in hydroclimate over time. Lower average $\delta^{18}O_{calcite}$ during the mid-Holocene (RS1 growth period) suggests that there was more precipitation than during the late Holocene. Trace element ratios with a lack of evidence for PCP (despite the presence of PCP in present-day RS) also support a wetter mid-Holocene, as the aquifer may have been too wet for PCP to occur in the epikarst.

These observations are consistent with results from previous sediment and stalagmite studies in Belize that found wetter, less variable mid-Holocene hydroclimate (e.g., Metcalfe et al., 2009; Pollock et al., 2016) in comparison to the later Holocene. Lacustrine records from the YP also showed higher mid-Holocene lake levels (e.g., Hodell et al., 1995; Whitmore et al., 1996), and a series of calcite rafts from other caves in the YP show progressive drying from 7,000 yr BP to the present (Kovacs et al., 2017). While it is possible that the difference in $\delta^{18}O$ between RS1 and Itzamna is not *solely* due to decreased precipitation amount, the similarity between our findings and published data suggests that the northeastern YP, like Belize and Guatemala, was wetter during the mid-Holocene than the late Holocene.

The apparent ~25-year lead/lag between Pollock et al. (2016) and RS1 is within age model uncertainty for both stalagmites, so it is possible that the two records are actually changing synchronously at a decadal scale. If there is indeed a lag between the major shifts in oxygen isotope ratios, that would indicate the presence of a precipitation control that first impacted the northern YP and did not affect the southern YP and Belize until later. Regional agreement among these paleoclimate records, across proxies and archives, within age model uncertainty suggests that the driver of increased precipitation amount and decreased precipitation variability is not isolated to this cave site or restricted to this short interval of the mid-Holocene. Instead, the driver(s) is at least regional in scale and persisted for a large portion of the mid-Holocene.

Furthermore, comparing RS1 to the sediment record from LPA (Wahl et al., 2014) showed that the $\delta^{18}O$ shifts seen in the southern YP between ~5,750 and 5,550 yr BP are reproducible at higher temporal resolution and are qualitatively similar to those found in a different archive from the northern YP. The coherence between the records further supports the use of $\delta^{18}O$ to reconstruct past hydroclimate in Mesoamerica.

Based on the longer records shown in Figure 6, it appears that RS1 captured a representative part of the mid-Holocene, not an extremely wet or variable period, so we suggest that the ~500-year-long RS1 record

applies to the whole mid-Holocene. We now explore potential drivers of increased precipitation amount and reduced variability in the mid-Holocene.

Increased precipitation amount is likely due (in part) to increased insolation seasonality during the mid-Holocene, which preferentially warmed North Atlantic summer SSTs, promoting increased YP precipitation via enhanced moisture transport by the CLLJ and a more northerly mean position of the Atlantic ITCZ. This link between North Atlantic SSTs and YP precipitation has been observed in the instrumental record and model simulations (Bhattacharya et al., 2017) and has been invoked to explain other observed proxy records (Pollock et al., 2016; Ridley et al., 2015; Wahl et al., 2014). Other work, however, also emphasizes the importance of the pressure gradient between the western tropical Atlantic and the eastern tropical Pacific in driving Mesoamerican precipitation variability in the late Holocene (Bhattacharya & Coats, 2020; Wahl et al., 2014), suggesting that wet mid-Holocene conditions in the YP may also have required relatively high SLP over the eastern tropical Pacific.

Increased tropical cyclone activity could have been partially responsible for higher YP precipitation in the mid-Holocene. Pausata et al. (2017) modeled tropical cyclone activity at 6,000 yr BP and demonstrated that increased seasonality, a vegetated Sahara, and a reduction in Saharan dust emissions could lead to an increase in tropical cyclones during the mid-Holocene, especially in the Caribbean. Under modern conditions, RS is impacted by a greater number of historical tropical cyclones but has less total summer precipitation than the Guatemala and Belize regions of the YP (Section 1). Therefore, an increase in tropical cyclones would have a larger impact on the northern YP than on the southern YP, potentially explaining why the δ^{18}O change appears larger in RS1 than in the records from the southern YP (Figure 6). We cannot resolve individual high-precipitation events in our record due to the nature of water infiltration into the karst at RS, so other types of archives would be better suited to specifically identify the impact of individual tropical cyclones in the YP during the mid-Holocene.

Lower precipitation variability during the mid-Holocene could be related to reduced ENSO variability. Several studies have shown that the mid-Holocene was a period of reduced ENSO variance compared to the late Holocene (Carré et al., 2014; Chen et al., 2016; Emile-Geay et al., 2016; Koutavas & Joanides, 2012; Koutavas et al., 2006). Summer CLLJ variability is thought to be linked to tropical Pacific variability (Muñoz et al., 2008), so decreased Pacific SST variability could lead to a more stable CLLJ, yielding the diminished precipitation variation we observe in RS1. Furthermore, previous modeling, monitoring, and proxy data have suggested that ENSO mean state influences tropical Atlantic cyclone formation (Elsner et al., 1999; Frappier et al., 2014; Lases-Hernandez et al., 2019; Medina-Elizalde, Polanco-Martínez, et al., 2016; Wu & Lau, 1992). Therefore, decreased ENSO variability during the mid-Holocene could reduce changes in the frequency of tropical cyclones, further decreasing the amplitude of precipitation variability in the YP.

Our study contributes to a wide range of work linking changes in Atlantic SSTs, including Atlantic Multidecadal Variability (AMV), to Caribbean and Gulf of Mexico hydroclimate (Alexander et al., 2014; Bhattacharya et al., 2017; Karmalkar et al., 2011; Knight et al., 2006; Winter et al., 2020). The high-resolution data presented here will allow for comparisons with SST reconstructions to better understand how future SST shifts will impact Central American hydroclimate. Instrumental, paleoclimate, and modeling data also support a link between AMV and hydroclimate over multiple other regions, including the North Atlantic (Knight et al., 2006), northeastern Brazil (Sutton & Hodson, 2005), African Sahel (Folland et al., 1986; Rowell et al., 1992), western Europe (Folland et al., 1986; Knight et al., 2006; Sutton & Hodson, 2005), and North America (Fensterer et al., 2012; Folland et al., 2001; Medina-Elizalde et al., 2017). Future work should examine whether paleoclimate records with decadal-scale resolution from these other regions also show reduced variance in the mid-Holocene relative to the late Holocene.

Regardless of the climate dynamics at play, the anomalous precipitation events (both those less than 20 years long and others that were 20–50 years long) observed in RS1 indicate significant multidecadal wet–dry cycles, much like there are in the present and late Holocene YP, despite the wetter, warmer climate state of the mid-Holocene. Thus, we expect similar, multidecadal droughts both under future climate warming and in other paleoclimate records from this region, including others that overlap with shifts in ancient Maya society.

5. Conclusions

In this study, we have presented a precisely dated, high-resolution, multiproxy YP paleoclimate record spanning a 456-year-long interval (5,721 ± 52 to 5,265 ± 130 yr BP) of the mid-Holocene. Results from this study suggest that multidecadal precipitation variations (both wet and dry) were a persistent feature in regional hydroclimate during the mid-Holocene, just as they were in the past 2,000 years, but with reduced amplitude. The record is consistent with previous observations of southern YP hydroclimate, which found increased precipitation in the mid-Holocene. High-resolution proxy sampling (1.3 years per sample) in RS1 also allowed us to detect anomalous precipitation events with durations of less than 20 years.

Because the mid-Holocene had a different climate mean state (more summer solar input and higher mean precipitation) than the late Holocene, we conclude that background climate can impact precipitation variability in the YP. We suggest that mid-Holocene reductions in ENSO and/or AMV variability, driven by altered seasonality, led to more stable precipitation patterns throughout the YP. As background climate changes under anthropogenic warming conditions, it will be important to examine changes in precipitation mean and variance indicated by climate models. Model simulations of future hydroclimate can be tested by comparing predicted variance at 6 kyr BP to that recorded in other proxy records and 6 kyr models. Given that the YP is already vulnerable to tropical cyclones and may also face decreased wet season precipitation in the future, it is critical for projections to be as accurate as possible. We suggest that the mid-Holocene offers an important test for model performance that can be used to assess the substantial disagreements between future projections in the region (Bhattacharya & Coats, 2020), providing improved confidence in climate adaptation strategies for its ~4 million residents.

This work presents the first record of stalagmite Mg/Ca and Sr/Ca ratios in the YP. Our results support the inclusion of trace element ratios in stalagmites that cover changes in ancient Maya civilization to provide additional climate information. These results are a step forward in YP paleo proxy interpretations and provide a better understanding of controls on precipitation amount and variability.

Data Availability Statement

Data generated in this study are available in the NOAA/WDS archive (https://www.ncdc.noaa.gov/paleo/study/29211) and supporting information. Data from Itzamna are available as supporting data in Medina-Elizalde, Burns, et al. (2016) and drip water data from Lases-Hernandez (2020) are available as tables within the thesis.

References

Akers, P. D., Brook, G. A., Railsback, L. B., Liang, F., Iannone, G., Webster, J. W., et al. (2016). An extended and higher-resolution record of climate and land use from stalagmite MC01 from Macal Chasm, Belize, revealing connections between major dry events, overall climate variability, and Maya sociopolitical changes. *Palaeogeography, Palaeoclimatology, Palaeoecology*, *459*, 268–288. https://doi.org/10.1016/j.palaeo.2016.07.007

Alexander, M. A., Halimeda Kilbourne, K., & Nye, J. A. (2014). Climate variability during warm and cold phases of the Atlantic Multidecadal Oscillation (AMO) 1871–2008. *Journal of Marine Systems*, *133*, 14–26.

Anderson, L., & Wahl, D. (2016). Two Holocene paleofire records from Peten, Guatemala: Implications for natural fire regime and prehispanic Maya land use. *Global and Planetary Change*, *138*, 82–92. https://doi.org/10.1016/j.gloplacha.2015.09.012

Appendini, C. M., Meza-Padilla, R., Abud-Russell, S., Proust, S., Barrios, R. E., & Secaira-Fajardo, F. (2019). Effect of climate change over landfalling hurricanes at the Yucatan Peninsula. *Climatic Change*, *157*, 469–482. https://doi.org/10.1007/s10584-019-02569-5

Aragón-Moreno, A. A., Islebe, G. A., & Torrescano-Valle, N. (2012). A ~3800-yr, high-resolution record of vegetation and climate change on the north coast of the Yucatan Peninsula. *Review of Palaeobotany and Palynology*, *178*, 35–42. https://doi.org/10.1016/j.revpalbo.2012.04.002

Bhattacharya, T., Chiang, J. C. H., & Cheng, W. (2017). Ocean–atmosphere dynamics linked to 800–1050 CE drying in Mesoamerica. *Quaternary Science Reviews*, *169*, 263–277. https://doi.org/10.1016/j.quascirev.2017.06.005

Bhattacharya, T., & Coats, S. (2020). Atlantic–Pacific gradients drive last millennium hydroclimate variability in Mesoamerica. *Geophysical Research Letters*, *47*, e2020GL088061. https://doi.org/10.1029/2020GL088061

Breitenbach, S. F. M., Rehfeld, K., Goswami, B., Baldini, J. U. L., Ridley, H. E., Kennett, D. J., et al. (2012). Constructing proxy records from age models (COPRA). *Climate of the Past*, *8*, 1765–1779. https://doi.org/10.5194/cp-8-1765-2012

Burns, S. J., Godfrey, L. R., Faina, P., McGee, D., Hardt, B., Ranivoharimanana, L., & Randrianasy, J. (2016). Rapid human-induced landscape transformation in Madagascar at the end of the first millennium of the Common Era. *Quaternary Science Reviews*, *134*, 92–99. https://doi.org/10.1016/j.quascirev.2016.01.007

Burns, S. J., Matter, A., Frank, N., & Mangini, A. (1998). Speleothem-based paleoclimate record from northern Oman. *Geology*, *26*(6), 499–502. https://doi.org/10.1130/0091-7613(1998)026<0499:SBPRFN>2.3.CO;2

Bush, M. B., Correa-Metrio, A. Y., Hodell, D. A., Brenner, M., Anselmetti, F. S., Ariztegui, D., et al. (2009). Re-evaluation of climate change in lowland central America during the last glacial maximum using new sediment cores from Lake Petén Itzá, Guatemala. In *Past climate variability in South America and surrounding regions. Developments in paleoenvironmental research* (pp. 113–128). Springer. https://doi.org/10.1007/978-90-481-2672-9_5

Carré, M., Sachs, J. P., Purca, S., Schauer, A. J., Braconnot, P., Falcón, R. A., et al. (2014). Holocene history of ENSO variance and asymmetry in the eastern tropical Pacific. *Science*, *345*(6200), 1045–1048. https://doi.org/10.1126/science.1252220

Chen, S., Hoffmann, S. S., Lund, D. C., Cobb, K. M., Emile-Geay, J., & Adkins, J. F. (2016). A high-resolution speleothem record of western equatorial Pacific rainfall: Implications for Holocene ENSO evolution. *Earth and Planetary Science Letters*, *442*, 61–71. https://doi.org/10.1016/j.epsl.2016.02.050

Cruz, F. W., Burns, S. J., Jercinovic, M., Karmann, I., Sharp, W. D., & Vuille, M. (2007). Evidence of rainfall variations in Southern Brazil from trace element ratios (Mg/Ca and Sr/Ca) in a Late Pleistocene stalagmite. *Geochimica et Cosmochimica Acta*, *71*, 2250–2263. https://doi.org/10.1016/j.gca.2007.02.005

Curtis, J. H., Hodell, D. A., & Brenner, M. (1996). Climate variability on the Yucatan Peninsula (Mexico) during the past 3500 years, and implications for Maya cultural evolution. *Quaternary Research*, *46*(1), 37–47. https://doi.org/10.1006/qres.1996.0042

Dansgaard, W. (1964). Stable isotopes in precipitation. *Tellus*, *16*, 436–468. https://doi.org/10.1111/j.2153-3490.1964.tb00181.x10.3402/tellusa.v16i4.8993

Dorale, J. A., Edwards, R. L., Ito, E., & Gonzalez, L. A. (1998). Climate and vegetation history of the midcontinent from 75 to 25 ka: A speleothem record from Crevice Cave, Missouri, USA. *Science*, *282*(5395), 1871–1874. https://doi.org/10.1126/science.282.5395.1871

Douglas, P. M. J., Pagani, M., Canuto, M. A., Brenner, M., Hodell, D. A., Eglinton, T. I., & Curtis, J. H. (2015). Drought, agricultural adaptation, and sociopolitical collapse in the Maya Lowlands. *Proceedings of the National Academy of Sciences of the United States of America*, *112*, 5607–5612. https://doi.org/10.1073/pnas.1419133112

Edwards, R. L., Chen, J. H., & Wasserburg, G. J. (1987). ^{238}U–^{234}U–^{230}Th–^{232}Th systematics and the precise measurement of time over the past 500,000 years. *Earth and Planetary Science Letters*, *81*(2–3), 175–192. https://doi.org/10.1016/0012-821X(87)90154-3

Elsner, J. B., Kara, A. B., & Owens, M. A. (1999). Fluctuations in North Atlantic hurricane frequency. *Journal of Climate*, *12*(2), 427–437. https://doi.org/10.1175/1520-0442(1999)012<0427:FINAHF>2.0.CO;2

Emile-Geay, J., Cobb, K. M., Carré, M., Braconnot, P., Leloup, J., Zhou, Y., et al. (2016). Links between tropical Pacific seasonal, interannual and orbital variability during the Holocene. *Nature Geoscience*, *9*, 168–173. https://doi.org/10.1038/ngeo2608

Fairchild, I. J., Baker, A., Borsato, A., Frisia, S., Hinton, R. W., McDermott, F., & Tooth, A. F. (2001). Annual to sub-annual resolution of multiple trace-element trends in speleothems. *Journal of the Geological Society*, *158*(5), 831–841. https://doi.org/10.1144/jgs.158.5.831

Fairchild, I. J., Borsato, A., Tooth, A. F., Frisia, S., Hawkesworth, C. J., Huang, Y., et al (2000). Controls on trace element (Sr–Mg) compositions of carbonate cave waters: Implications for speleothem climatic records. *Chemical Geology*, *166*(3–4), 255–269. https://doi.org/10.1016/S0009-2541(99)00216-8

Farfán, L. M., D'Sa, E. J., Liu, K.-b., & Rivera-Monroy, V. H. (2014). Tropical cyclone impacts on coastal regions: The case of the Yucatán and the Baja California Peninsulas, Mexico. *Estuaries and Coasts*, *37*(6), 1388–1402. https://doi.org/10.1007/s12237-014-9797-2

Fensterer, C., Scholz, D., Hoffmann, D., Spötl, C., Pajón, J. M., & Mangini, A. (2012). Cuban stalagmite suggests relationship between Caribbean precipitation and the Atlantic Multidecadal Oscillation during the past 1.3 ka. *The Holocene*, *22*(12), 1405–1412. https://doi.org/10.1177/0959683612449759

Folland, C. K., Colman, A. W., Rowell, D. P., & Davey, M. K. (2001). Predictability of northeast Brazil rainfall and real-time forecast skill, 1987–98. *Journal of Climate*, *14*(9), 1937–1958. https://doi.org/10.1175/1520-0442(2001)014<1937:PONBRA>2.0.CO;2

Folland, C. K., Palmer, T. N., & Parker, D. E. (1986). Sahel rainfall and worldwide sea temperatures, 1901–85. *Nature*, *320*, 602–607. https://doi.org/10.1038/320602a0

Frappier, A. B., Pyburn, J., Pinkey-Drobnis, A. D., Wang, X., Corbett, D. R., & Dahlin, B. H. (2014). Two millennia of tropical cyclone-induced mud layers in a northern Yucatán stalagmite: Multiple overlapping climatic hazards during the Maya Terminal Classic "megadroughts". *Geophysical Research Letters*, *41*, 5148–5157. https://doi.org/10.1002/2014GL059882

Frappier, A. B., Sahagian, D., Carpenter, S. J., González, L. A., & Frappier, B. R. (2007). Stalagmite stable isotope record of recent tropical cyclone events. *Geology*, *35*(2), 111–114. https://doi.org/10.1130/G23145A.1

Genty, D., Baker, A., Massault, M., Proctor, C., Gilmour, M., Pons-Branchu, E., & Hamelin, B. (2001). Dead carbon in stalagmites: Carbonate bedrock paleodissolution vs. ageing of soil organic matter. Implications for ^{13}C variations in speleothems. *Geochimica et Cosmochimica Acta*, *65*(20), 3443–3457. https://doi.org/10.1016/S0016-7037(01)00697-4

Genty, D., Blamart, D., Ghaleb, B., Plagnes, V., Causse, C., Bakalowicz, M., et al. (2006). Timing and dynamics of the last deglaciation from European and North African δ^{13}C stalagmite profiles-comparison with Chinese and South Hemisphere stalagmites. *Quaternary Science Reviews*, *25*(17–18), 2118–2142. https://doi.org/10.1016/j.quascirev.2006.01.030

Giannini, A., Kishnir, Y., & Cane, M. A. (2000). Interannual variability of Caribbean rainfall, ENSO, and the Atlantic Ocean. *Journal of Climate*, *32*(18), 297–311. https://doi.org/10.1175/1520-0442(2000)013<0297:IVOCRE>2.0.CO;2

Grinsted, A., Moore, J. C., & Jevrejeva, S. (2004). Application of the cross wavelet transform and wavelet coherence to geophysical time series. *Nonlinear Processes in Geophysics*, *11*, 561–566. https://doi.org/10.5194/npg-11-561-2004

Gutiérrez-Ayala, L. V., Torrescano-Valle, N., & Islebe, G. A. (2012). Reconstrucción paleoambiental del Holoceno tardío de la reserva Los Petenes, Península de Yucatán. *Revista Mexicana de Ciencias Geológicas*, *29*(3), 749–763. http://www.scielo.org.mx/pdf/rmcg/v29n3/v29n3a17.pdf

Hellstrom, J., McCulloch, M., & Stone, J. (1998). A detailed 31,000-year record of climate and vegetation change, from the isotope geochemistry of two New Zealand speleothems. *Quaternary Research*, *50*, 167–178. https://doi.org/10.1006/qres.1998.1991

Hodell, D. A., Brenner, M., Curtis, J. H., Medina-González, R., Ildefonso-Chan Can, E., Albornaz-Pat, A., & Guilderson, T. P. (2005). Climate change on the Yucatan Peninsula during the little ice age. *Quaternary Research*, *63*, 109–121. https://doi.org/10.1016/j.yqres.2004.11.004

Hodell, D. A., Curtis, J. H., & Brenner, M. (1995). Possible role of climate in the collapse of Classic Maya civilization. *Nature*, *375*(6530), 391–394. https://doi.org/10.1038/375391a0

Islebe, G. A., Torrescano-Valle, N., Aragón-Moreno, A. A., Vela-Peláez, A. A., & Valdez-Hernández, M. (2018). The paleoanthropocene of the Yucatán Peninsula: Palynological evidence of environmental change. *Boletín De La Sociedad Geológica Mexicana*, *70*(1), 49–60. https://doi.org/10.18268/bsgm2018v70n1a3

Karmalkar, A. V., Bradley, R. S., & Diaz, H. F. (2011). Climate change in Central America and Mexico: Regional climate model validation and climate change projections. *Climate Dynamics*, *37*, 605–629. https://doi.org/10.1007/s00382-011-1099-9

Kaufman, D., McKay, N., Routson, C., Erb, M., Dätwyler, C., Sommer, P. S., et al. (2020). Holocene global mean surface temperature, a multi-method reconstruction approach. *Scientific Data*, *7*(1), 201. http://dx.doi.org/10.1038/s41597-020-0530-7

Kennett, D. J., Breitenbach, S. F. M., Aquino, V. V., Asmerom, Y., Awe, J., Baldini, J. U. L., et al. (2012). Development and disintegration of maya political systems in response to climate change. *Science*, *338*(6108), 788–791. https://doi.org/10.1126/science.1226299

Knapp, K. R., Diamond, H. J., Kossin, J. P., Kruk, M. C., & Schreck, C. J. (2018). International Best Track Archive for Climate Stewardship (IBTrACS) project, version 4. NOAA National Centers for Environmental Information. https://doi.org/10.25921/82ty-9e16

Knapp, K. R., Kruk, M. C., Levinson, D. H., Diamond, H. J., & Neumann, C. J. (2010). The International Best Track Archive for Climate Stewardship (IBTrACS). *Bulletin of the American Meteorological Society*, *91*, 363–376. https://doi.org/10.1175/2009BAMS2755.1

Knight, J. R., Folland, C. K., & Scaife, A. A. (2006). Climate impacts of the Atlantic multidecadal oscillation. *Geophysical Research Letters*, *33*, L17706. https://doi.org/10.1029/2006GL026242

Koutavas, A., deMenocal, P. B., Olive, G. C., & Lynch-Stieglitz, J. (2006). Mid-Holocene El Niño–Southern Oscillation (ENSO) attenuation revealed by individual foraminifera in eastern tropical Pacific sediments. *Geology*, *34*(12), 993–996. https://doi.org/10.1130/G22810A.1

Koutavas, A., & Joanides, S. (2012). El Niño–Southern Oscillation extrema in the Holocene and Last Glacial Maximum. *Paleoceanography*, *27*, PA4208. https://doi.org/10.1029/2012PA002378

Kovacs, S. E., Reinhardt, E. G., Chatters, J. C., Rissolo, D., Schwarcz, H. P., Collins, S. V., et al. (2017). Calcite raft geochemistry as a hydrological proxy for Holocene aquifer conditions in Hoyo Negro and Ich Balam (Sac Actun Cave System), Quintana Roo, Mexico. *Quaternary Science Reviews*, *175*, 97–111. https://doi.org/10.1016/j.quascirev.2017.09.006

Lachniet, M. S., Asmerom, Y., Polyak, V., & Bernal, J. P. (2017). Two millennia of Mesoamerican monsoon variability driven by Pacific and Atlantic synergistic forcing. *Quaternary Science Reviews*, *155*, 100–113. https://doi.org/10.1016/j.quascirev.2016.11.012

Lachniet, M. S., Burns, S. J., Piperno, D. R., Asmerom, Y., Polyak, V., Moy, C. M., & Christenson, K. (2004). A 1500-year El Niño/Southern Oscillation and rainfall history for the Isthmus of Panama from speleothem calcite. *Journal of Geophysical Research*, *109*, D20117. https://doi.org/10.1029/2004JD004694

Landsea, C. W., & Franklin, J. L. (2013). Atlantic hurricane database uncertainty and presentation of a new database format. *Monthly Weather Review*, *141*, 3576–3592. https://doi.org/10.1175/MWR-D-12-00254.1

Larson, J., Zhou, Y., & Higgins, R. W. (2005). Characteristics of landfalling tropical cyclones in the United States and Mexico: Climatology and interannual variability. *Journal of Climate*, *18*(8), 1247–1262. https://doi.org/10.1175/JCLI3317.1

Lases-Hernandez, F. (2020). Characterization of geochemical and environmental processes controlling the stable isotope and trace element composition of drip water and farmed calcite in Río Secreto karst cave, located in the Yucatán Peninsula, México (Doctoral thesis). Retrieved from TESIUNAM. http://oreon.dgbiblio.unam.mx/F/3VJHE3YNUCP47152DLDQHQ7GQ6AQ8V5HQKNMDDT3M6YXT-KLB2K-16483?func=full-set-set&set_number=012438&set_entry=000001&format=999

Lases-Hernandez, F., Medina-Elizalde, M., Burns, S., & DeCesare, M. (2019). Long-term monitoring of drip water and groundwater stable isotopic variability in the Yucatán Peninsula: Implications for recharge and speleothem rainfall reconstruction. *Geochimica et Cosmochimica Acta*, *246*, 41–59. https://doi.org/10.1016/j.gca.2018.11.028

Laskar, J., Robutel, P., Joutel, F., Gastineau, M., Correia, A. C. M., & Levrard, B. (2004). A long-term numerical solution for the insolation quantities of the Earth. *Astronomy and Astrophysics*, *428*(1), 261–285. https://doi.org/10.1051/0004-6361:20041335

Lechleitner, F. A., Breitenbach, S. F. M., Rehfeld, K., Ridley, H. E., Asmerom, Y., Prufer, K. M., et al. (2017). Tropical rainfall over the last two millennia: Evidence for a low-latitude hydrologic seesaw. *Scientific Reports*, *7*(1), 45809. https://doi.org/10.1038/srep45809

Lewis, S. C., Gagan, M. K., Ayliffe, L. K., Zhao, J., Hantoro, W. S., Treble, P. C., et al. (2011). High-resolution stalagmite reconstructions of Australian–Indonesian monsoon rainfall variability during Heinrich stadial 3 and Greenland interstadial 4. *Earth and Planetary Science Letters*, *303*(1–2), 133–142. https://doi.org/10.1016/j.epsl.2010.12.048

Marcott, S. A., Shakun, J. D., Clark, P. U., & Mix, A. C. (2013). A reconstruction of regional and global temperature for the past 11,300 years. *Science*, *339*(6124), 1198–1201. https://doi.org/10.1126/science.1228026

Marsicek, J., Shuman, B. N., Bartlein, P. J., Shafer, S. L., & Brewer, S. (2018). Reconciling divergent trends and millennial variations in Holocene temperatures. *Nature*, *554*, 92–96. https://doi.org/10.1038/nature25464

McGee, D., Donohoe, A., Marshall, J., & Ferreira, D. (2014). Changes in ITCZ location and cross-equatorial heat transport at the Last Glacial Maximum, Heinrich Stadial 1, and the mid-Holocene. *Earth and Planetary Science Letters*, *390*, 69–79. https://doi.org/10.1016/j.epsl.2013.12.043

Medina-Elizalde, M., Burns, S. J., Lea, D. W., Asmerom, Y., von Gunten, L., Polyak, V., et al. (2010). High resolution stalagmite climate record from the Yucatán Peninsula spanning the Maya terminal classic period. *Earth and Planetary Science Letters*, *298*(1–2), 255–262. https://doi.org/10.1016/j.epsl.2010.08.016

Medina-Elizalde, M., Burns, S. J., Polanco-Martinez, J., Lases-Hernández, F., Bradley, R., Wang, H.-C., & Shen, C.-C. (2017). Synchronous precipitation reduction in the American Tropics associated with Heinrich 2. *Scientific Reports*, *7*, 11216. https://doi.org/10.1038/s41598-017-11742-8

Medina-Elizalde, M., Burns, S. J., Polanco-Martínez, J. M., Beach, T., Lases-Hernández, F., Shen, C.-C., & Wang, H.-C. (2016). High-resolution speleothem record of precipitation from the Yucatan Peninsula spanning the Maya Preclassic Period. *Global and Planetary Change*, *138*, 93–102. https://doi.org/10.1016/j.gloplacha.2015.10.003

Medina-Elizalde, M., Polanco-Martínez, J. M., Lases-Hernández, F., Bradley, R., & Burns, S. (2016). Testing the "tropical storm" hypothesis of Yucatan Peninsula climate variability during the Maya Terminal Classic Period. *Quaternary Research*, *86*, 111–119. https://doi.org/10.1016/j.yqres.2016.05.006

Mendez, M., & Caetano, E. (2007). UNAM monthly precipitation and maximum and minimum temperature analyses for Mexico and surroundings. IRI/LDEO Climate Data Library. Retrieved from https://iridl.ldeo.columbia.edu/SOURCES/.UNAM/

Mestas-Nuñez, A. M., Enfield, D. B., & Zhang, C. (2007). Water vapor fluxes over the Intra-Americas Sea: Seasonal and interannual variability and associations with rainfall. *Journal of Climate*, *20*(9), 1910–1922. https://doi.org/10.1175/JCLI4096.1

Metcalfe, S., Breen, A., Murray, M., Furley, P., Fallick, A., & McKenzie, A. (2009). Environmental change in northern Belize since the latest Pleistocene. *Journal of Quaternary Science*, *24*, 627–641. https://doi.org/10.1002/jqs.1248

Muñoz, E., Busalacchi, A. J., Nigam, S., & Ruiz-Barradas, A. (2008). Winter and summer structure of the Caribbean low-level jet. *Journal of Climate*, *21*(6), 1260–1276. https://doi.org/10.1175/2007JCLI1855.1

Pausata, F. S. R., Emanuel, K. A., Chiacchio, M., Diro, G. T., Zhang, Q., Sushama, L., et al. (2017). Tropical cyclone activity enhanced by Sahara greening and reduced dust emissions during the African Humid Period. *Proceedings of the National Academy of Sciences of the United States of America*, *114*(24), 6221–6226. https://doi.org/10.1073/pnas.1619111114

Pollock, A., van Beynen, P. E., DeLong, K. L., Polyak, V., Asmerom, Y., & Reeder, P. (2016). A mid-Holocene paleoprecipitation record from Belize. *Palaeogeography, Palaeoclimatology, Palaeoecology*, *463*, 103–111. https://doi.org/10.1016/j.palaeo.2016.09.021

Richey, J. N., Poore, R. Z., Flower, B. P., Quinn, T. M., & Hollander, D. J. (2009). Regionally coherent Little Ice Age cooling in the Atlantic Warm Pool. *Geophysical Research Letters*, *36*, L21703. https://doi.org/10.1029/2009GL040445

Ridley, H. E., Asmerom, Y., Baldini, J. U. L., Breitenbach, S. F. M., Aquino, V. V., Prufer, K. M., et al. (2015). Aerosol forcing of the position of the intertropical convergence zone since ad 1550. *Nature Geoscience*, *8*(3), 195–200. https://doi.org/10.1038/ngeo2353

Roberts, M. S., Smart, P. L., & Baker, A. (1998). Annual trace element variations in a Holocene speleothem. *Earth and Planetary Science Letters*, *154*(1–4), 237–246. https://doi.org/10.1016/S0012-821X(97)00116-7

Rosenmeier, M. F., Hodell, D. A., Brenner, M., Curtis, J. H., & Guilderson, T. P. (2002). A 4000-year lacustrine record of environmental change in the Southern Maya Lowlands, Petén, Guatemala. *Quaternary Research*, *57*(2), 183–190. https://doi.org/10.1006/qres.2001.2305

Rowell, D. P., Folland, C. K., Maskell, K., Owen, J. A., & Ward, M. N. (1992). Modeling the influence of global sea surface temperatures on the variability and predictability of seasonal Sahel rainfall. *Geophysical Research Letters*, *19*(9), 905–908. https://doi.org/10.1029/92GL00939

Roy, P. D., Torrescano-Valle, N., Islebe, G. A., & Gutiérrez-Ayala, L. V. (2017). Late Holocene hydroclimate of the western Yucatan Peninsula (Mexico). *Journal of Quaternary Science*, *32*(8), 1112–1120. https://doi.org/10.1002/jqs.2988

Sinclair, D. J., Banner, J. L., Taylor, F. W., Partin, J., Jenson, J., Mylroie, J., et al. (2012). Magnesium and strontium systematics in tropical speleothems from the Western Pacific. *Chemical Geology*, *294–295*, 1–17. https://doi.org/10.1016/j.chemgeo.2011.10.008

Stahle, D. W., Burnette, D. J., Diaz, J. V., Heim, R. R., Fye, F. K., Paredes, J. C., et al. (2012). Pacific and Atlantic influences on Mesoamerican climate over the past millennium. *Climate Dynamics*, *39*(6), 1431–1446. https://doi.org/10.1007/s00382-011-1205-z

Steponaitis, E., Andrews, A., McGee, D., Quade, J., Hsieh, Y.-T., Broecker, W. S., et al. (2015). Mid-Holocene drying of the U.S. Great Basin recorded in Nevada speleothems. *Quaternary Science Reviews*, *127*, 174–185. https://doi.org/10.1016/j.quascirev.2015.04.011

Sutton, R. T., & Hodson, D. L. R. (2005). Atlantic Ocean forcing of North American and European summer climate. *Science*, *309*(5731), 115–118. https://doi.org/10.1126/science.1109496

Taylor, S. R., & McLennan, S. M. (1985). *The continental crust: Its composition and evolution. An examination of the geochemical record preserved in sedimentary rocks.* Blackwell Scientific.

Tremaine, D. M., & Froelich, P. N. (2013). Speleothem trace element signatures: A hydrologic geochemical study of modern cave dripwaters and farmed calcite. *Geochimica et Cosmochimica Acta*, *121*, 522–545. https://doi.org/10.1016/j.gca.2013.07.026

Tremaine, D. M., Froelich, P. N., & Wang, Y. (2011). Speleothem calcite farmed in situ: Modern calibration of δ^{18}O and δ^{13}C paleoclimate proxies in a continuously-monitored natural cave system. *Geochimica et Cosmochimica Acta*, *75*(17), 4929–4950. https://doi.org/10.1016/j.gca.2011.06.005

Vuille, M., Bradley, R. S., Healy, R., Werner, M., Hardy, D. R., Thompson, L. G., & Keimig, F. (2003). Modeling δ^{18}O in precipitation over the tropical Americas: 2. Simulation of the stable isotope signal in Andean ice cores. *Journal of Geophysical Research*, *108*(6), 4175. https://doi.org/10.1029/2001JD002039

Wahl, D., Byrne, R., & Anderson, L. (2014). An 8700 year paleoclimate reconstruction from the southern Maya lowlands. *Quaternary Science Reviews*, *103*, 19–25. https://doi.org/10.1016/j.quascirev.2014.08.004

Whitmore, T. J., Brenner, M., Curtis, J. H., Dahlin, B. H., & Leyden, B. W. (1996). Holocene climatic and human influences on lakes of the Yucatan Peninsula, Mexico: An interdisciplinary, palaeolimnological approach. *The Holocene*, *6*(3), 273–287. https://doi.org/10.1177/095968369600600303

Winter, A., Zanchettin, D., Lachniet, M., Vieten, R., Pausata, F. S. R., Ljungqvist, F. C., et al. (2020). Initiation of a stable convective hydroclimatic regime in Central America circa 9000 years BP. *Nature Communications*, *11*(1), 716. https://doi.org/10.1038/s41467-020-14490-y

Wong, C. I., & Breecker, D. O. (2015). Advancements in the use of speleothems as climate archives. *Quaternary Science Reviews*, *127*, 1–18. https://doi.org/10.1016/j.quascirev.2015.07.019

Wu, G., & Lau, N.-C. (1992). A GCM simulation of the relationship between tropical-storm formation and ENSO. *Monthly Weather Review*, *120*(6), 958–977. https://doi.org/10.1175/1520-0493(1992)120<0958:AGSOTR>2.0.CO;2